Transient buoyant convection in a ventilated box filled with a porous medium

by

Ali Moradi

A thesis submitted in partial fulfillment of the requirements for the degree of

Master of Science

Department of Mechanical Engineering
University of Alberta

Abstract

We examine the transient evolution of a negatively buoyant, laminar plume in an emptying filling box containing a uniform porous medium. In the long time limit, $\tau \to \infty$, the box is partitioned into two uniform layers of different densities. However, the approach towards steady state is characterized by a lower contaminated layer that is continuously stratified. The presence of this continuous stratification poses nontrivial analytical challenges; we nonetheless demonstrate that it is possible to derive meaningful bounds on the range of possible solutions particularly in the limit of large μ, where μ represents the ratio of the draining to filling timescales. The validity of our approach is confirmed by drawing comparisons against the free turbulent plume case where, unlike with porous media plumes, an analytical solution that accounts for the time-variable continuous stratification of the lower layer is available (Baines & Turner, *J. Fluid Mech.*, vol. 37, 1969, pp. 51–80; Germeles, *J. Fluid Mech.*, vol. 71, 1975, pp. 601–623). A separate component of our study considers time-variable forcing where the laminar plume source strength changes abruptly with time. When the source is turned on and off with a half-period, $\Delta\tau$, the depth and reduced gravity of the contaminated layer oscillate between two

extrema after the first few cycles. Different behaviour is seen when the source is merely turned up or down. For instance, a change of the source reduced gravity leads to a permanent change of interface depth, which is a qualitative point of difference from the free turbulent plume case.

Preface

This thesis is an original work by Ali Moradi under supervision of Dr. Morris R. Flynn. The work incorporated into Chapter 2 has been submitted for publication as A. Moradi and M. R. Flynn, "Emptying filling boxes – free turbulent vs. laminar porous media plumes" to the *Journal of Fluid Mechanics*.

This dissertation is lovingly dedicated to my mother, Maryam Zaree. Her support, encouragement, and constant love have sustained me throughout my life.

Acknowledgements

I would like to express my deepest appreciation and thanks to my supervisor, Dr. Morris R. Flynn, for his continuous support of my research, his guidance, patience, motivation, and enthusiasm. Without his support and guidance this dissertation would not have been possible. *Thank you.*

There are way too many people inside and outside the university who have supported, motivated, and helped me through this process. *Thank you all.*

Financial support was provided by the Faculty of Graduate Studies and Research, the Natural Sciences and Engineering Research Council (NSERC) of Canada (Discovery Grants Program) and Carbon Management Canada.

Contents

List of Figures

List of Symbols

$\bar{g}'$	average reduced gravity of the contaminated layer
χ_1	ratio of the source buoyancy fluxes
χ_2	ratio of the source volume fluxes
$\Delta\tau$	half-period of a cyclic source
δ	dimensionless average reduced gravity of the contaminated layer
δ_{ss}	steady state dimensionless average reduced gravity of the contaminated layer
μ	ratio of the draining to the filling timescales
μ_c	critical μ beyond which the well-mixed model can predict an overshoot
ν	kinematic viscosity
ϕ	porosity
ρ	density of the contaminated layer
ρ_a	external ambient density

τ dimensionless time

τ_{cr} dimensionless time beyond which the Germeles solution becomes bracketed

$\tau_{ss,wm}$ dimensionless time taken ti reach 99.9% of ξ_{ss} for the well-mixed model

ξ dimensionless interface depth of the contaminated layer

ξ_{over} maximum magnitude of the overshoot

ξ_{ss} steady state dimensionless depth of the contaminated layer

A cross-sectional area of the lower opening

$A^{\star}$ weighted area of the lower and upper openings

b depth of the lower opening

C_j constant obtained from the entrainment coefficient and source geometry

D solute dispersion coefficient

F_0 source buoyancy flux

g gravitational acceleration

g' reduced gravity of the contaminated layer

H total depth of the box

h depth of the contaminated layer

I integrated buoyancy of the contaminated layer

k	permeability of the box
k_f	permeability of the lower opening
Q_0	plume source volume flux
Q_p	plume volume flux
Q_{out}	outflow volume flux
S	cross-sectional area of the box
t	time
T_d	draining timescale
T_f	filling timescale
V	volume of the contaminated layer
x	vertical coordinate
x_0	virtual origin correction

Chapter 1

Introduction

High Reynolds number density driven flow from a discrete source, be it a point- or a line-source, have been broadly investigated since the seminal work of Morton *et al.* (1956). Morton *et al.* (1956) employed the equations for mass, momentum and buoyancy conservation in order to develop an analytical model to describe a turbulent plume in an infinite stratified or unstratified ambient. The main assumptions that Morton *et al.* (1956) used are as follows: (i) the profiles of the plume vertical velocity and buoyancy are similar at every height, (ii) the rate of the entrainment of external ambient fluid is proportional to the vertical velocity of the plume, and (iii) the fluids are incompressible and the flow is Boussinesq, i.e. the density differences are taken into account only when they are multiplied by gravitational acceleration. Practically speaking, the Boussinesq approximation implies that ascending plumes are dynamically equivalent to descending plumes; much of our focus in the present work is on the latter category of flow. The Morton *et al.* (1956) model has been successfully employed in studying manifold topics, such as bubble plumes (McDougall, 1978; Wüest *et al.*, 1992) volcanic erup-

tions (Woods, 1988), hydrothermal plumes (Speer & Rona, 1989), oil leakage from the deep ocean (Adalsteinsson *et al.*, 2011) as well as various other natural (and industrial) flows (Woods, 2010).

By adapting the Morton *et al.* (1956) equations, Baines & Turner (1969) studied the flow evolution of turbulent plume inside a closed box. They thereby developed a one-dimensional model in which the details of the horizontal motion of the discharged plume fluid were neglected. In such a "filling box" flow with a descending plume, the plume, upon reaching the bottom of the box, spreads out laterally and forms a non-turbulent layer of discharged plume fluid (i.e. contaminated fluid) whose thickness steady increases with time. Baines & Turner (1969) found that in the case of an ideal source having zero source volume flux, the contaminated layer interface (or "first front") reaches the top of the box/elevation of the source asymptotically at large time. Baines & Turner's description has subsequently been applied to describe numerous environmental and industrial problems, for instance, seafloor lava eruptions (Speer & Marshall, 1995; Bush & Woods, 1999), the filling of a room with smoke during fires (Kaye & Hunt, 2007), and architectural exchange flows (Nabi & Flynn, 2013). A numerical scheme based on the formulation of Baines & Turner (1969) to determine the evolution of the stratified layer was developed by Germeles (1975). Germeles's work was motivated by the need to better understand mixing in chemical storage tanks. More precisely, Germeles (1975) focused on minimizing the likelihood of "rollover" in tanks containing liquefied natural gas (LNG). Rollover may occur upon the injection of new LNG having

a different composition and temperature of the resident material already present in the tank. Germeles's algorithm, which we describe in more detail in Appendices A and B, has since been adopted to investigate filling box (Worster & Huppert, 1983; Caulfield & Woods, 2002) and emptying filling box flow (Bolster *et al.*, 2008; Bolster & Caulfield, 2008).

Linden *et al.* (1990) first used the term "emptying filling box" in their study of turbulent plumes in a ventilated box. An emptying filling box is connected to an infinite external ambient via upper and lower openings. Due to differences in the internal and external hydrostatic pressure distributions, a ventilation flow naturally arises whereby, in the case of a negatively buoyant plume, discharged plume fluid exits the box through the lower opening to be replaced, in turn, by external ambient fluid, which flows through the upper opening. Emptying filling box models have been broadly adapted to describe various ventilation problems, for example, natural ventilation of one- (Linden *et al.*, 1990; Linden, 1999) and two-zone buildings (Lin & Linden, 2002; Flynn & Caulfield, 2006), transient ventilation dynamics (Kaye & Hunt, 2004) and the possibility of multiple steady states (Holford & Hunt, 2000), and the oscillatory behaviour of general non-Boussinesq emptying filling box flows (Vauquelin, 2015).

Recently, there has been a theoretical and experimental development in studying filling and emptying filling box flows in control volumes filled with porous media. In this circumstance, the turbulent plume is replaced with one that falls at low Reynolds number

through a uniform or nonuniform porous medium. For the case of a porous media plume, the plume cross sectional area increases as the plume falls as a result of molecular or mechanical dispersion unlike a free turbulent plume where the broadening is driven by engulfment via turbulent eddies. Roes *et al.* (2014) studied the steady state behaviour of an emptying filling box in a control volume filled with a uniform (and isotropic) porous medium. Consistent with Linden *et al.* (1990), they found that as the system approaches steady state, the box is partitioned into two regions of different densities. Moreover, the plume volume flux at the interface depth equals the outflow volume flux. The transient behaviour of filling box flows in boxes filled with porous media was investigated by Sahu & Flynn (2015, 2016*b*) for the case of uniform porous media and by Sahu & Flynn (2016*a*) for the case of a nonuniform medium consisting of two distinct layers of different permeabilities. While porous media plumes are not unusual phenomena in nature, the study of such flows remains incomplete, particularly in connection with filling box-type flows. Problems of this sort are of particular interest in hydrology and related disciplines, such as

(i) The dissolution of dense non-aqueous phase liquids into potable groundwater. Infiltration of dense non-aqueous phase liquids (DNAPL) such as creosote, coal tar and chlorinated solvents, through the unsaturated zone between the surface and the water table and then into potable groundwater supplies is considered as one of the most dangerous forms of groundwater contamination. This contamination is, in turn, the cause of major health problems (Kueper *et al.*,

2003). In order to gain a better understanding of the process of DNAPL contamination, it is first necessary to develop of equations describing the DNAPL plume volume flux and concentration.

(ii) The geological sequestration of anthropogenically-produced CO_2 e.g. in deep saline aquifers or in depleted oil and gas reservoirs. To date, this strategy for mitigating climate change has been restricted to large-scale industrial emitters e.g. coal-fired power plants and requires the compression of the CO_2 to a supercritical state (Bickle, 2009). In turn, CO_2 capture and geological storage involves a diverse set of physical, chemical and geological phenomena. With respect to fluid mechanics, note that CO_2, even when compressed to a supercritical state, remains more buoyant (i.e. less dense) than aquifer brine. There is therefore a tendency for the sc-CO_2 plume to rise through the geological formation. This, in turn, opens up the alarming possibility of a flow to surface event e.g. through a network of fissures or an old or improperly sealed oil and gas well (Bolster, 2014). Even in the presence of cap rock of high structural integrity, fluid mechanics might also impact the horizontal motion of the CO_2 plume relative to the ambient fluid (Dentz & Tartakovsky, 2009), the dissolution of CO_2 into this other fluid phase (Kneafsey & Pruess, 2010), and the downward flow of the resulting mixture into the underlying ambient as a result of buoyant convection (Riaz *et al.*, 2006). In order to consider the geological sequestration of CO_2 as a safe and cost-effective strategy to reduce atmospheric emissions of greenhouse gases, flow timescales and reservoir capacity must also be considered (in addition to a

myriad of questions concerning operating vs. capital cost, long-term liability, etc.).

(iii) Geothermal energy recovery. Considering the unsustainability of fossil fuels and their negative effects on the climate, there has been enhanced interest in developing and improving efficiency of alternate energy sources (MacKay, 2009). For instance, the Alberta government has recently introduced the "Albertas climate leadership plan" according to which up to 30% of Alberta's electricity generation will be from renewable sources by 2030. Geothermal energy recovery is a method of withdrawing energy from hot underground aquifers for either heating applications or electricity generation. The extraction of hot fluid from underground is, except in particular locales such as Iceland, accompanied by a subsequent re-injection of spent water, whose high salinity precludes surface disposal. The important technical considerations in harnessing geothermal energy are the recovery factor, which is the ratio of recovered thermal energy to that injected, and the recovered energy (or temperature) level and its variations (Sauty *et al.*, 1982). The injection and extraction of the fluids, and the physical properties of the reservoir, e.g. the porosity and permeability, are major parameters in determining the technological and economic feasibility of geothermal operations. Filling box and emptying filling box concepts can be applied when determining the practicability of a geothermal energy recovery project. Specifically, because geothermal energy recovery is operated on a cyclic basis, the time periodic forcing of an emptying box flow may provide valuable information.

Due to a lack of previous study of porous media plumes in ventilated boxes, this thesis is devoted to an improved understanding of time-dependent flows in an emptying filling box filled with a porous medium. In an emptying filling box, the contaminated layer is continuously stratified, but the strength of this stratification diminishes over time. Ultimately, the system attains steady state in such a way that the box is partitioned into two regions of different uniform densities. (The plume fluid and ambient are assumed to be fully miscible one within the other and have the same viscosity.) For the case of turbulent free plumes, the emptying filling box equations can be numerically solved to high precision. However, an analogue technique for the case of porous media plumes has not been developed yet. Thus, the corresponding "exact" solution (consisting of the solution of the 1D integral model summarized in Appendix A) cannot be obtained. In this study, we show that, even in the absence of such a model, the exact solution can be bracketed by considering two limiting cases at least when t is not too small. Our approach is substantiated by drawing extensive comparisons with the analogue case of a free turbulent plume flow. In this way, we identify the qualitative and quantitative similarities between these two categories of filling box model, one thoroughly studied over the past two decades, the other very much less so.

The rest of the discussion is organized as follows: Chapter 2 contains the essential results but without exhaustive elaboration. Rather, particulars are purposefully relegated to the appendices where many important details are carefully described. In section

2.1, we formulate the problem with reference to boxes that are either filled with or devoid of porous media. Solutions derived assuming an initially uncontaminated box are then presented and discussed in section 2.2. In section 2.3, the criteria for the contaminated layer to overshoot its steady state depth is outlined. Time-varying sources are then considered in sections 2.4 and 2.5. A detailed comparison between the free turbulent and porous media plume cases is presented in section 2.6. Section 2.7 discusses conclusions of this work. Chapter 3 summarizes the key findings of this study and presents topics for future investigation. A brief description of, and the MATLAB codes relevant to, Germeles's algorithm, which is used to find the exact solution of point-source free turbulent plumes, are given in Appendices A and B, respectively. Appendix C discusses the formulation applicable to a box devoid of porous media in which the viscous dissipation due to flow through in the lower fissure cannot be ignored. The formulation pertinent to a ventilated filling box containing a porous medium and having a variable cross-sectional area is given in Appendix D. Finally, a brief discussion of the stability of second-order linear homogeneous differential equations systems is presented in Appendix E.

Chapter 2

Emptying filling boxes – free turbulent vs. laminar porous media plumes

2.1 Theory – basic formulation

We begin by investigating the flow dynamics of a ventilated filling box that is either filled with, or devoid of, a porous medium. A pair of schematics illustrating these two cases are presented in figure 2.1, which indicates the position of the negatively-buoyant plumes relative to the lower openings[1]. These openings, along with the upper opening of figure 2.1a and the open top of figure 2.1b, connect the box interior to an infinite external ambient of density ρ_a. Note that the difference of opening configuration along the upper boundary reflects the fact that porous media flows in nature, such as those mentioned in the previous section, are, in general, more realistically

[1]In the porous media flow literature, such an opening is more typically referred to as a "fissure". Likewise, in the natural ventilation literature, the term "vent" is often applied. Because a major focus of this study is to draw a comparison between the porous media and free turbulent plume cases, we prefer to use the more generic term "opening" throughout. We do so on the understanding that viscous dissipation respectively is and is not dynamically significant in the porous media and free turbulent flow scenarios. Appendix C discusses the formulation applicable to a box devoid of porous media in which the viscous dissipation is not negligible in the lower fissure.

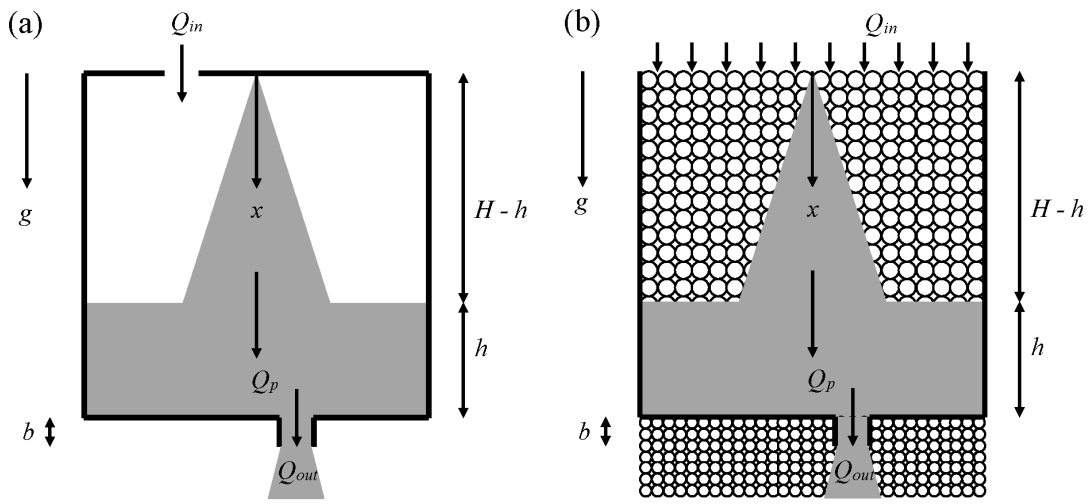

Figure 2.1: Schematic of emptying filling boxes devoid of (panel a) and filled with (panel b) porous media. Each box contains a single negatively buoyant plume, which is supposed to originate from either a point- or a line-source.

represented by an open upper boundary.

Applying conservation of volume and buoyancy to the lower contaminated layer leads to

$$\frac{\mathrm{d}V}{\mathrm{d}t} = Q_p - Q_{out}, \tag{2.1}$$

$$\frac{\mathrm{d}(SI)}{\mathrm{d}t} = F_0 - Q_{out} g'|_{x=H}, \tag{2.2}$$

where V is the volume of the contaminated layer. In the case of a box devoid of porous media, $V = Sh$ where S and h denote the cross-sectional area of the box (independent of depth[2]) and the depth of the lower contaminated layer, respectively. By contrast, if the box is filled with a porous medium, $V = \phi Sh$ in which ϕ is the porosity or void fraction. Meanwhile, F_0 is the source buoyancy flux and the integrated buoyancy of the contaminated layer, is defined

[2]An overview of formulation relevant to a ventilated box filled with a porous media and having a variable cross-sectional area is given in Appendix D.

as

$$I = \int_{H-h}^{H} g' \mathrm{d}x, \tag{2.3}$$

in which H is the total depth of the box and g' is the reduced gravity of the contaminated layer, i.e.

$$g' = g\frac{\rho - \rho_a}{\rho_a}. \tag{2.4}$$

Here ρ is the density of the contaminated layer, which we allow to vary in time, t, and in the vertical direction. We assume a Boussinesq flow so that density differences are dynamically important only when they multiply gravitational acceleration. Finally, Q_p and Q_{out} denote, respectively, the plume volume flux at the level of the interface and the volumetric rate of outflow through the lower opening. Expressions for Q_p and Q_{out} are as follows (see for instance Kaye & Hunt, 2004; Roes *et al.*, 2014):

free turbulent plume:

$$Q_p = C_j F_0^{1/3}(x + x_0)^j, \qquad Q_{out} = A^\star \sqrt{I + g'|_{x=H} b}, \tag{2.5}$$

point-source porous media plume:

$$Q_p = 8\pi D\phi(x + x_0), \qquad Q_{out} = \frac{Ak_f}{\nu b}(I + g'|_{x=H} b), \tag{2.6}$$

line-source porous media plume:

$$Q_p = \left(\frac{36 D\phi F_0 k(x + x_0)\Lambda^2}{\nu}\right)^{1/3}, Q_{out} = \frac{Ak_f}{\nu b}(I + g'|_{x=H} b). \tag{2.7}$$

In (2.5) j depends on the plume geometry, i.e. $j = 5/3$ and $j = 1$ correspond to point- and line-source plumes, respectively. Furthermore, the constant C_j is obtained from the entrainment coefficient and source geometry, x is the vertical coordinate measured relative

to the source, x_0 is the virtual origin correction for non-ideal plumes having a finite source volume flux, $A^\star$ is the weighted area of the lower and upper openings, and b is the depth of lower opening. In (2.6) and (2.7), D denotes the solute dispersion coefficient which we assume to be spatially-invariant (Wooding, 1963). The problem of a spatially-variable D has been studied, among many others, by Sahu & Flynn (2015, 2016*b*) whose expressions for Q_p could just as easily be used instead of the above formulas. Moreover, A and k_f denote, respectively, the cross-sectional area and permeability of the lower opening, ν is the kinematic viscosity, k denotes the permeability of the box, and Λ is the depth of the line-source into the page. The virtual origin corrections in (2.5)-(2.7) are respectively defined as

$$\text{free turbulent plume: } x_0 = \left(\frac{Q_0}{C_j F_0^{1/3}}\right)^{1/j}, \tag{2.8}$$

$$\text{point-source porous media plume: } x_0 = \frac{Q_0}{8\pi D\phi}, \tag{2.9}$$

$$\text{line-source porous media plume: } x_0 = \frac{Q_0^3\nu}{36 D\phi F_0 k\Lambda^2}, \tag{2.10}$$

where $Q_0\,(>0)$ is the plume source volume flux.

We define the average reduced gravity of the contaminated layer as $\bar{g}' = I/h$ and use (2.5)-(2.7) to rewrite (2.1) and (2.2) as

$$S\frac{\mathrm{d}h}{\mathrm{d}t} = C_j F_0^{1/3}(H - h + x_0)^j - A^\star\sqrt{\bar{g}'h + g'|_{x=H}b}, \tag{2.11}$$

$$S\frac{\mathrm{d}(\bar{g}'h)}{\mathrm{d}t} = F_0 - A^\star\sqrt{\bar{g}'h + g'|_{x=H}b}\,g'|_{x=H}, \tag{2.12}$$

for a free turbulent plume, and as

$$\phi S\frac{\mathrm{d}h}{\mathrm{d}t} = 8\pi D\phi(H-h+x_0) - \frac{Ak_f}{\nu b}(\bar{g}'h + g'|_{x=H}b), \tag{2.13}$$

$$\phi S\frac{\mathrm{d}(\bar{g}'h)}{\mathrm{d}t} = F_0 - \frac{Ak_f}{\nu b}(\bar{g}'h + g'|_{x=H}b)g'|_{x=H}, \tag{2.14}$$

for a point-source porous media plume, and finally as

$$\begin{aligned}\phi S\frac{\mathrm{d}h}{\mathrm{d}t} =& \left(\frac{36D\phi F_0 k\Lambda^2}{\nu}\right)^{1/3}(H-h+x_0)^{1/3} \\ &- \frac{Ak_f}{\nu b}(\bar{g}'h + g'|_{x=H}b),\end{aligned} \tag{2.15}$$

$$\phi S\frac{\mathrm{d}(\bar{g}'h)}{\mathrm{d}t} = F_0 - \frac{Ak_f}{\nu b}(\bar{g}'h + g'|_{x=H}b)g'|_{x=H}, \tag{2.16}$$

for a line-source porous media plume. We also introduce the following dimensionless parameters

$$\xi = \tfrac{h}{H} \quad \text{and} \quad \left|\begin{array}{ll} \delta = \bar{g}'\frac{C_j H^j}{F_0^{2/3}} & \text{(free turbulent plume)} \\ \delta = \bar{g}'\frac{8\pi D\phi H}{F_0} & \text{(point-source porous media plume)} \\ \delta = \bar{g}'\left(\frac{36D\phi k H\Lambda^2}{F_0^2\nu}\right)^{1/3} & \text{(line-source porous media plume)}\end{array}\right., \tag{2.17}$$

where ξ and δ represent a dimensionless interface depth and a dimensionless average reduced gravity of the contaminated layer, respectively. For an emptying filling box problem, two timescales are

typically considered (Kaye & Hunt, 2004)

free turbulent plume:

$$T_d = \frac{SC_j^{1/2}H^{(j+1)/2}}{A^\star F_0^{1/3}}, \quad T_f = \frac{S}{C_j F_0^{1/3} H^{(j-1)}}, \tag{2.18}$$

point-source porous media plume:

$$T_d = \frac{8\pi D\phi^2\nu S H^2}{A k_f F_0}, \quad T_f = \frac{S}{8\pi D}, \tag{2.19}$$

line-source porous media plume:

$$T_d = \left(\frac{36 D\phi^4\nu^2 k\Lambda^2 S^3 H^4}{A^3 k_f^3 F_0^2}\right)^{1/3}, \quad T_f = \left(\frac{S^3\phi^2 H^2\nu}{36 D F_0 k\Lambda^2}\right)^{1/3}, \tag{2.20}$$

where T_f is the filling timescale assuming an ideal plume with source buoyancy flux F_0. Meanwhile, T_d is the draining timescale and is proportional to the time taken for a contaminated layer spanning the entire depth of the box to drain completely through the lower opening.

Having introduced the draining and filling timescales, we can now non-dimensionalize time according to $t = \sqrt{T_d T_f}\tau$. Equations (2.11) and (2.12) may then be rewritten for a free turbulent plume as

$$\frac{\mathrm{d}\xi}{\mathrm{d}\tau} = \sqrt{\mu}\left(1 - \xi + \frac{x_0}{H}\right)^j - \frac{1}{\sqrt{\mu}}\sqrt{\delta\xi + \delta|_{x=H}\frac{b}{H}}, \tag{2.21}$$

$$\frac{\mathrm{d}\delta}{\mathrm{d}\tau} = \frac{\sqrt{\mu}}{\xi}\left[1 - \delta\left(1 - \xi + \frac{x_0}{H}\right)^j\right] + \frac{\delta - \delta|_{x=H}}{\sqrt{\mu}}\sqrt{\frac{\delta\xi + \delta|_{x=H} b/H}{\xi^2}}. \tag{2.22}$$

The analogue, and similar looking, expressions for a laminar plume

falling through a porous medium are given by

$$\frac{\mathrm{d}\xi}{\mathrm{d}\tau} = \sqrt{\mu}\left(1-\xi+\frac{x_0}{H}\right)^k - \frac{1}{\sqrt{\mu}b/H}\left(\delta\xi+\delta|_{x=H}\frac{b}{H}\right), \tag{2.23}$$

$$\frac{\mathrm{d}\delta}{\mathrm{d}\tau} = \frac{\sqrt{\mu}}{\xi}\left[1-\delta\left(1-\xi+\frac{x_0}{H}\right)^k\right] + \frac{\delta-\delta|_{x=H}}{\sqrt{\mu}b/H}\left(\frac{\delta\xi+\delta|_{x=H}b/H}{\xi}\right), \tag{2.24}$$

where $k = 1$ and $k = 1/3$ correspond to point- and line-source plumes, respectively. In (2.21)-(2.24), μ is the ratio of the draining to the filling timescales. More explicitly,

$$\text{free turbulent plume: } \mu = \frac{C_j^{3/2}H^{(3j-1)/2}}{A^\star}, \tag{2.25}$$

$$\text{point-source porous media plume: } \mu = \frac{(8\pi D\phi)^2\nu H^2}{Ak_fF_0}, \tag{2.26}$$

$$\text{line-source porous media plume: } \mu = \left[\frac{(36D\phi)^2\nu k^2\Lambda^4H^2}{A^3k_f^3F_0}\right]^{1/3}. \tag{2.27}$$

As noted by Bolster *et al.* (2008) for the case of free turbulent plumes, the ratio of the latter to the former terms on the right hand sides of (2.22) and (2.24) are proportional to μ. Hence, for large μ, these latter terms, which specifically incorporate the stratification of the contaminated layer, become negligible compared to the former terms. A well-mixed model in which the latter terms are identically zero, is therefore a reliable approximation of the "exact" solution for large μ.

From (2.21)-(2.24) it is elementary to determine the steady state depth, ξ_{ss}, and reduced gravity, δ_{ss}, of the contaminated layer either

by solving

$$\mu^2 \left(1 - \xi_{ss} + \frac{x_0}{H}\right)^{3j} = \left(\xi_{ss} + \frac{b}{H}\right), \tag{2.28}$$

$$\delta_{ss} = \frac{1}{\left(1 - \xi_{ss} + \frac{x_0}{H}\right)^j}, \tag{2.29}$$

for a free turbulent plume, or

$$\mu \left(1 - \xi_{ss} + \frac{x_0}{H}\right)^{2k} \left(\frac{b}{H}\right) = \left(\xi_{ss} + \frac{b}{H}\right), \tag{2.30}$$

$$\delta_{ss} = \frac{1}{\left(1 - \xi_{ss} + \frac{x_0}{H}\right)^k}, \tag{2.31}$$

for a porous media plume. Furthermore, from (2.28) and (2.30) we can determine the range of μ for which ξ assumes a physical value of between 0 and 1. To wit

$$\text{free turbulent plume: } \frac{\sqrt{b/H}}{\sqrt{(1 + x_0/H)^{3j}}} < \mu < \frac{\sqrt{1 + b/H}}{(x_0/H)^{3j}}, \tag{2.32}$$

$$\text{porous media plume: } \frac{1}{(1 + x_0/H)^{2k}} < \mu < \frac{1 + b/H}{(b/H)(x_0/H)^{2k}}. \tag{2.33}$$

For μ smaller than the lower bound, the draining capacity of the box is much larger than the filling capacity of the source so that a contaminated layer is never realized. On the other hand, for μ larger than the upper bound, the outflow from the lower opening cannot balance the source volume flux and contaminated fluid therefore occupies the entirety of the box; hence, a ventilation flow is not obtained.

In order to derive bounds on the range of possible solutions for the depth and reduced gravity of the contaminated layer, we consider two limiting cases. In the former, the lower layer is, in

spite of the possible presence of stratification, assumed to be well-mixed, i.e. the density is assumed to be spatially-uniform within the contaminated layer. Hence, the latter terms from the right-hand sides of (2.22) and (2.24) disappear. In the bookend opposite limiting case (hereafter referred to as the "approximate stratified model"), the density of the lower layer at the bottom of the box, which is unknown in case of porous media plumes, is assumed equal to the plume density at the level of the interface. This plume density, which we express in terms of the reduced gravity as $g'_p(x = H - h) = F_0/Q_p$, is the largest possible density that can be achieved within the contaminated layer whether or not the interface is stationary. Accordingly the factor $\delta|_{x=H}$ that appears in (2.21)-(2.24) is replaced with $1/\left(1 - \xi + x_0/H\right)^j$ for free turbulent plumes and $1/\left(1 - \xi + x_0/H\right)^k$ for porous media plumes.

So as to validate the legitimacy of the above approach, we apply the Germeles (1975) numerical technique to the free turbulent plume problem (2.21-2.22) to confirm that Germeles's "exact" filling box solution is bounded by the above limiting cases, at least when τ is not small. A comparison of model output is presented in figure 2.2, which shows the Germeles's exact filling box, well-mixed, and approximate stratified model solutions for canonical conditions, i.e. $\mu = 6.2$ and $x_0/H = b/H = 0$. Also included in figure 2.2a are data corresponding to the numerical simulations of Kaye *et al.* (2009), whose results were shown to agree very well with a series of small-scale laboratory experiments and theoretical models – see e.g. their figure 12. Shortly after "turning on" the source, figure 2.2

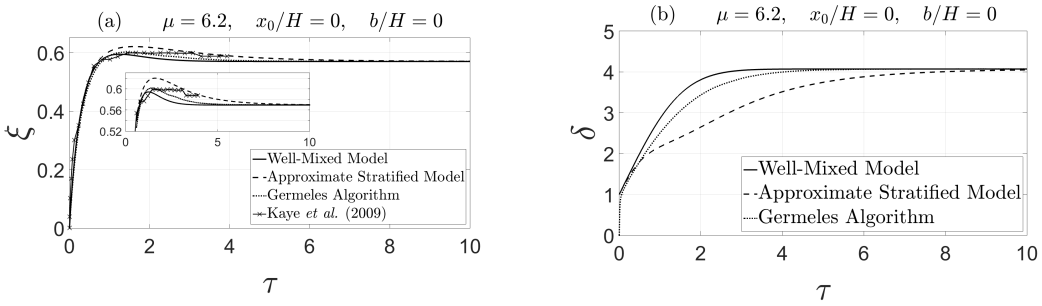

Figure 2.2: Evolution of the contaminated layer non-dimensional depth (panel a) and reduced gravity (panel b) calculated from Germeles (1975), the well-mixed model given by (2.21) and (2.22) with spatially-uniform δ, and the approximate stratified model given by (2.21) and (2.22) with $\delta|_{x=H}$ specified using the plume density at the level of the ambient interface. Also included is the evolution of the contaminated layer depth as extracted from figure 12 of Kaye *et al.* (2009). Here we assume an ideal point-source free turbulent plume with $x_0/H = 0$; moreover, $b/H = 0$ and $\mu = 6.2$.

indicates that the Germeles's solution becomes bracketed by those of the well-mixed and approximate stratified models. The initial discrepancy is due to the fact that in our numerical solutions of (2.21) and (2.22) the non-dimensional reduced gravity of the contaminated layer can never start from a value less than unity, i.e. in the aforementioned limiting cases the initial conditions are given by

$$\xi = 0, \quad \text{and} \quad \delta = \frac{1}{\left(1 + \frac{x_0}{H}\right)^j} \quad \text{at} \quad \tau = 0\,. \tag{2.34}$$

By contrast, the initial conditions for the Germeles (1975) algorithm assuming an ambient that is initially unstratified read $\xi = 0$ and $\delta = 0$ at $\tau = 0$. Hence, it takes some finite, but generally small, time for the system to evolve to the point that the Germeles's solution becomes bracketed. Elaborating on this point, figure 2.3 shows τ_{cr} for an ideal point-source plume with $b/H = 0$. Initially, τ_{cr} increases

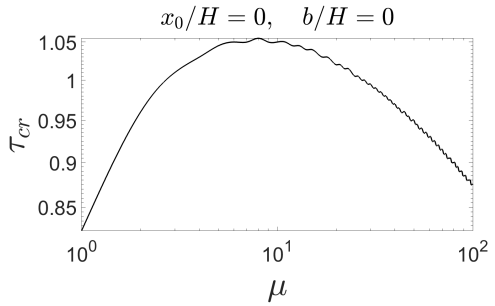

Figure 2.3: Non-dimensional time needed for the Germeles solution to become bounded the well-mixed and approximate stratified models. We consider here an ideal point-source plume with $b/H = 0$. Qualitatively similar results (not shown) are obtained for other plume configurations.

with μ; the maximum τ_{cr} corresponds to the maximum overshoot of contaminated layer depth, which is discussed in further detail in the following sections. Thereafter, as μ increases, the contaminated layer deepens more rapidly; hence, τ_{cr} decreases with μ. Note finally that, in the following sections where we study a cyclic or time-variable buoyancy source, the exact solution is bounded for all τ when we start from a non-zero contaminated layer depth.

Of course, figure 2.2 presents results for a relatively classical problem, namely an emptying filling box for a box devoid of porous media, rather than the more novel problem of a laminar, porous media plume in a ventilated box. To reiterate, our motivation for revisiting such a classical problem is that it gives us good confidence that a similar approach of bounding the exact solution can be applied when considering porous media convection where, as already highlighted, no analogue to the Germeles (1975) algorithm has ever been derived. Following on from the previous discussion, this confidence is based on the strong similarities between (2.21-2.22) and (2.23-

2.24) which, in turn, follows from a judicious non-dimensionalization of the relevant governing equations. In summary, and although an exact solution is unavailable for the flow of figure 2.1b, we expect such a solution to be bounded by the appropriate limiting cases of (2.23) and (2.24); these bounds become increasingly sharp in the limit of large μ. Note finally that the bounds are little influenced by the effects of ambient diffusion/dispersion because (2.3) depends on the integral of the density difference rather than its vertical distribution. As an example, if one were to allow for some intermingling of contaminated and uncontaminated fluid parcels across the ambient interface (as has been done for filling boxes devoid of porous media by Baines, 1983 and Kaye *et al.*, 2010), the outflux would not change. Thus the neglect of ambient diffusion/dispersion, which is formally valid for sufficiently large $Q_p\sqrt{t/D\phi}/S$, is not a major limitation of the analysis to follow.

2.2 Initial transient

From figure 2.2 and the discussion thereof, we expect to be able to bracket exact solutions to (2.23) and (2.24) provided τ is not too small. On this basis, we now proceed to solve these equations using the aforementioned assumptions so as to infer the true behavior of porous media filling box flows. For the case where the initial interior density is the ambient density, we take $\tau = 0$ as the moment when the plume first touches the bottom of the box. Therefore, similar

to (2.34), the initial conditions read

$$\xi = 0, \quad \text{and} \quad \delta = \frac{1}{\left(1 + \frac{x_0}{H}\right)^k} \quad \text{at} \quad \tau = 0. \tag{2.35}$$

Figure 2.4 shows the evolution of ξ and δ for ideal point-source free turbulent and porous media plumes with $b/H = 0.1$[3]. When μ is small, the contaminated layer is highly stratified. Dense fluid continuously drains from the bottom of the box and therefore the time rate of increase of the average density of the contaminated layer is small compared to cases where μ is large and the contaminated layer has a more or less uniform density profile. Hence, the outflow volume flux, which depends on this average density, increases comparatively slowly and the contaminated layer initially thickens quickly. Consequently, the contaminated layer first reaches then exceeds its steady state depth. Over time, ξ relaxes back to this steady state value as the filling and draining of the contaminated layer become balanced. (It should be noted that while the contaminated layer depth initially rises quickly, the approach toward steady state takes longer compared to the case of larger μ.) On the other hand, when μ is large, there is, as noted before, relatively little vertical variation in the density of the contaminated layer. Now, however, the filling timescale is smaller than the draining timescale. Therefore, an overshoot of contaminated layer depth is again observed. We defer till section 2.6 a quantitative comparison of the maximum overshoots for small and large μ. Suffice it to say for now that (i)

[3]Because the evolution of ξ and δ in the line-source case is qualitatively similar to the behavior seen in the point-source case, the former set of figures is not shown for the sake of brevity. In a similar spirit, and in sections 5-7, whenever the results for point- and line-source plumes are qualitatively similar, only the figures for point-source plumes will be presented.

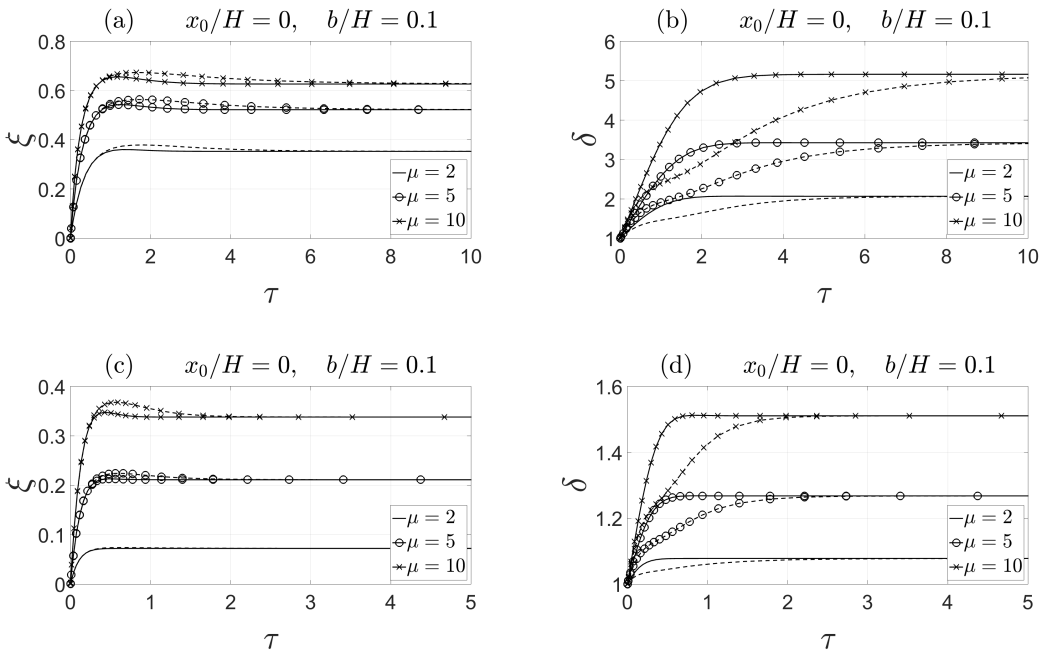

Figure 2.4: Ideal point-source free turbulent and porous media plumes with $\mu = \{2, 5, 10\}$ and $b/H = 0.1$. (a, b) Free turbulent plumes and (c, d) porous media plumes. The solid and dashed curves correspond to the well-mixed and approximate stratified models, respectively.

the overshoot is, in magnitude, comparable for the free turbulent and porous media plume cases, but, (ii) the steady state depth of the contaminated layer is greater in the free turbulent plume case for the same μ (figure 2.4). This difference can be explained by comparing the latter terms from the right-hand sides of (2.21) and (2.23) which describe the outflow volume flux. Due to the difference in the exponents, and for fixed μ, x_0/H and b/H, the outflow volume flux is smaller for a box devoid of porous media. As a result, the steady state depth and reduced gravity of the contaminated layer are both larger when the plume is of free turbulent type. Note finally that with the approximate stratified model, we can predict

the overshoot in the contaminated layer depth for both small and large μ. In the case of the well-mixed model, by contrast, overshoot requires that a threshold value of μ is first exceeded – see Kaye & Hunt (2004) and the discussion of the next section. An overshoot in the contaminated layer depth may be important for very large μ where the contaminated layer spans almost the entire box. In this case, an overshoot may result in a backflow of the contaminated fluid though the upper opening.

Figures 2.5 and 2.6 respectively show the effects of changing x_0/H and b/H on the evolution of the contaminated layer depth and reduced gravity. As confirmed by the former figure, increasing x_0/H results in an increase in the contaminated layer depth and a decrease in its reduced gravity for both free turbulent and porous media plumes. Meanwhile increasing the depth of the opening increases the hydrostatic draining capacity of filling boxes devoid of porous media. This, in turn, results in a decrease in the contaminated layer depth and reduced gravity. However, in case of a box filled with a porous medium, outflow is dominated by viscous drag and increasing the lower opening depth decreases, rather than increases, Q_{out} – see (2.6) and (2.7). Thus, the contaminated layer depth and reduced gravity increase with b/H.

2.3 Overshoot criteria

In order to compute, for the case of a well-mixed contaminated layer, the value of μ at which overshoot first occurs for given x_0/H

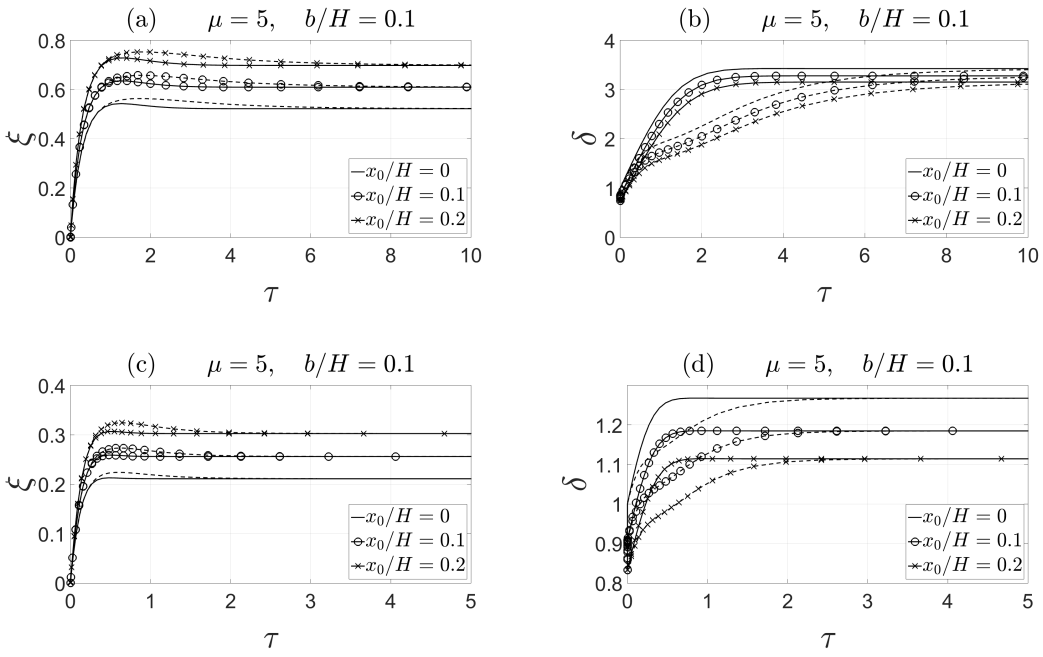

Figure 2.5: Point-source free turbulent and porous media plumes with $\mu = 5$, $x_0/H = \{0, 0.1, 0.2\}$ and $b/H = 0.1$. (a, b) Free turbulent plumes and (c, d) porous media plumes. The solid and dashed curves correspond to the well-mixed and approximate stratified models, respectively.

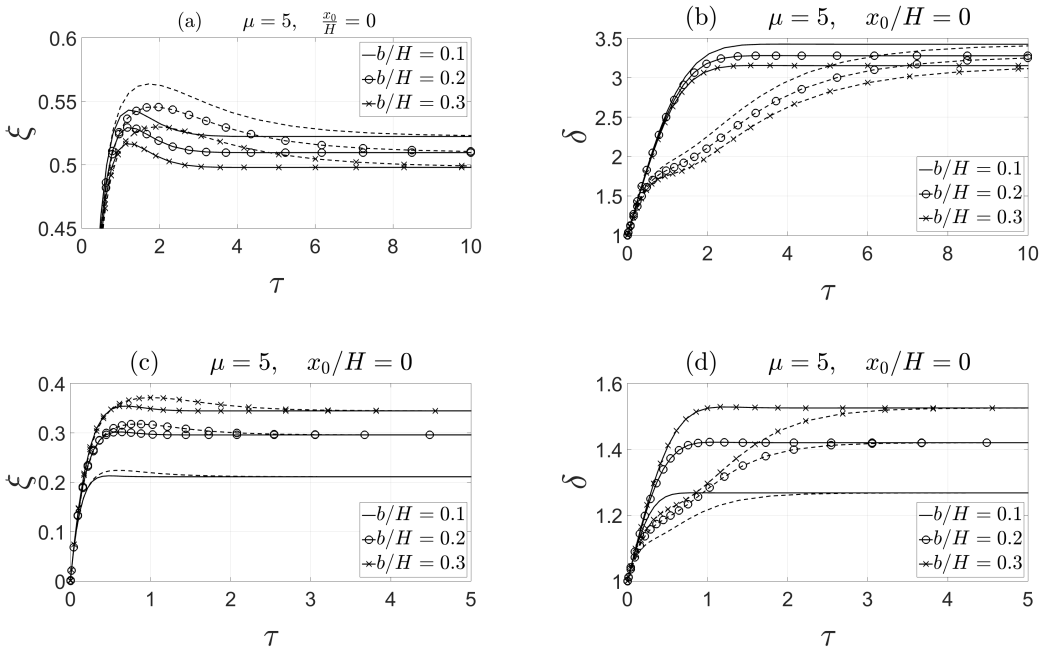

Figure 2.6: Ideal point-source free turbulent and porous media plumes with $\mu = 5$ and $b/H = \{0.1, 0.2, 0.3\}$. (a, b) Free turbulent plumes and (c, d) porous media plumes. The solid and dashed curves correspond to the well-mixed and approximate stratified models, respectively.

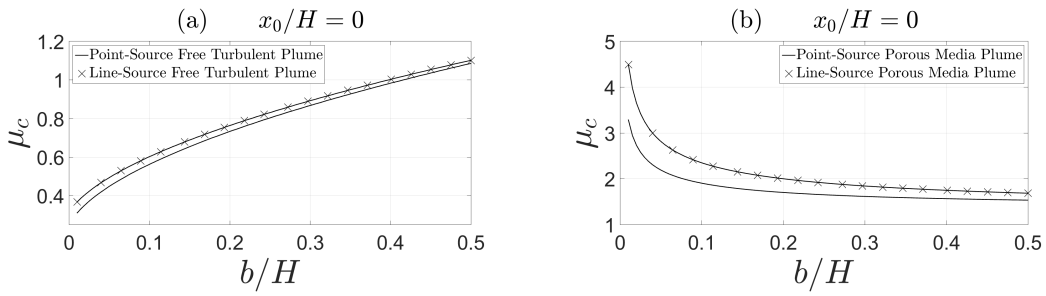

Figure 2.7: μ_c for ideal free turbulent and porous media plumes as functions of b/H. (a) Free turbulent plumes and (b) porous media plumes.

and b/H, we linearize (2.21-2.22) and (2.23-2.24) about their steady state values, i.e.

$$\begin{bmatrix} \dot{\xi} \\ \dot{\delta} \end{bmatrix} \approx \begin{bmatrix} \left.\frac{\partial \dot{\xi}}{\partial \xi}\right|_{\delta=\delta_{ss},\xi=\xi_{ss}} & \left.\frac{\partial \dot{\xi}}{\partial \delta}\right|_{\delta=\delta_{ss},\xi=\xi_{ss}} \\ \left.\frac{\partial \dot{\delta}}{\partial \xi}\right|_{\delta=\delta_{ss},\xi=\xi_{ss}} & \left.\frac{\partial \dot{\delta}}{\partial \delta}\right|_{\delta=\delta_{ss},\xi=\xi_{ss}} \end{bmatrix} \begin{bmatrix} \xi - \xi_{ss} \\ \delta - \delta ss \end{bmatrix}. \tag{2.36}$$

Following Kaye & Hunt (2004), we draw an analogy with a mass-spring-damper system, i.e. the system is overdamped when the above matrix has two distinct real eigenvalues and is underdamped when the eigenvalues are complex conjugates[4]. For given x_0/H and b/H, we numerically determine μ_c, the critical value of μ, corresponding to the boundary between an over- and underdamped system. Figure 2.7 shows μ_c for ideal free turbulent and porous media plumes as functions of b/H.

To reiterate, in the case of a box devoid of porous media, increasing the depth of the lower opening results in an increase in the hydrostatic pressure difference between inside and outside, which, in turn, increases the outflow of contaminated fluid. Thus, for the contaminated layer to overshoot, the filling capacity of the box should

[4]For more information, see Appendix E.

likewise increase to compensate, i.e. the filling timescale should decrease. It is no surprise then that an increase in b/H corresponds to an increase in μ_c in figure 2.7a. When the box is filled with porous media, however, (2.6) and (2.7) indicate that the outflow volume flux is inversely proportional to the depth of the lower opening. Therefore, increasing b/H in figure 2.7b results in a decrease in μ_c.

2.4 Transient source turned on and off

Consider now a situation where the plume source is sequentially turned on and off with a half-period of $\Delta\tau$. When the plume source is off, contaminated fluid continues to be discharged from the bottom of the box. As a consequence, the lower layer depth decreases monotonically in time until the source is again turned on. If the contaminated layer drains completely, i.e. if $\Delta\tau$ is sufficiently large, the box then consists of uniform ambient fluid just as with the presumed initial condition. For $\Delta\tau$ less than this critical value, the contaminated layer remains of finite thickness; its reduced gravity equals the value at the instant the source was turned off.

Figure 2.8 shows the evolution of ξ and δ for ideal point-source free turbulent and porous media plumes with $\mu = 10$, $b/H = 0.1$, and $\Delta\tau = 0.25$. If $\Delta\tau$ is smaller than the non-dimensional time required for the system to approach steady state, ξ_{ss} and δ_{ss} will never be realized regardless of the number of cycles. Rather, after a few cycles, the depth of the lower layer oscillates between two extrema whose values depend on the magnitude of $\Delta\tau$ in addition to

μ, x_0/H, and b/H (figures 2.8a and 2.8b). Consistent with the discussion of the previous paragraph and for sufficiently large $\Delta\tau$, the lower extrema corresponds to a box devoid of contaminated fluid (figures 2.8c and 2.8d). Also, consistent with our previous discussions, the time rate of increase of the contaminated layer depth is greater for the approximate stratified model compared to the well-mixed model. Hence, for the period when the source is on, the contaminated layer reaches a greater depth and correspondingly it takes longer for the contaminated fluid to drain out of the box for the period when the source is off.

2.5 Transient source turned up or down

Building on the material of the previous section, we now consider a limited increase or decrease in the source buoyancy flux or volume flux. Thus the source buoyancy flux might change from an initial value of F_0 to $F_0 + \Delta F$ or the source volume flux might change from an initial value of Q_0 to $Q_0 + \Delta Q$. Note that ΔF and ΔQ can be either positive or negative quantities but, by assumption, $F_0 + \Delta F > 0$ and $Q_0 + \Delta Q > 0$. Note also that a change in Q is not supposed to result in a change in F and vice-versa, i.e. ΔQ and ΔF are assumed to be uncorrelated.

Given a final buoyancy flux $F_0 + \Delta F$ or a volume flux $Q_0 + \Delta Q$,

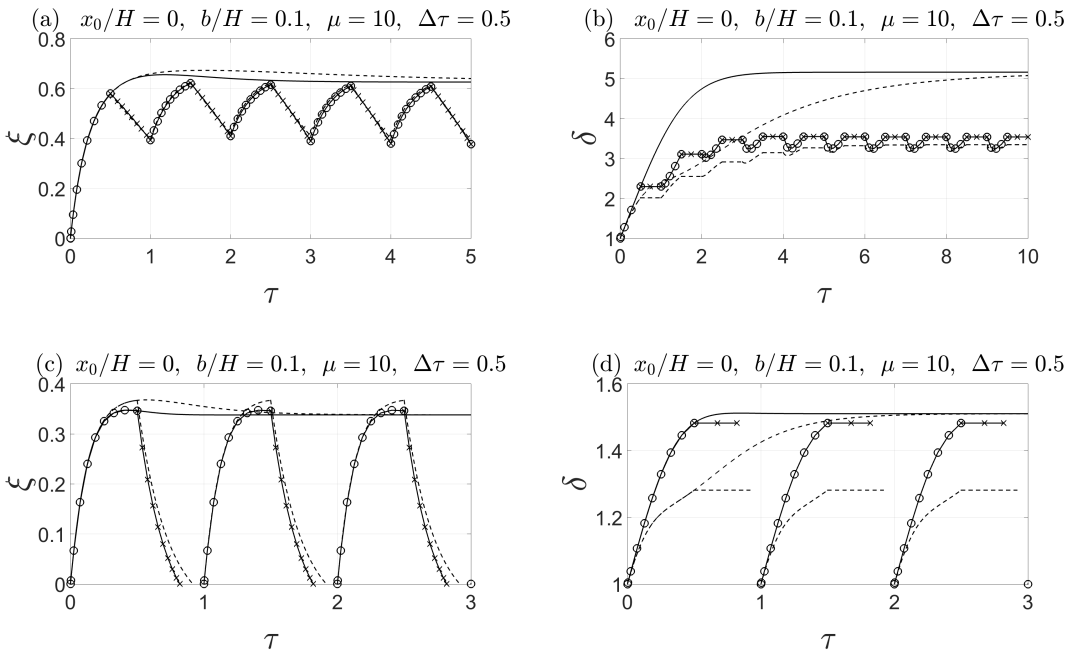

Figure 2.8: Ideal free turbulent and porous media plume responses to cyclic variations in the source conditions with $b/H = 0.1$, $\mu = 10$ and $\Delta\tau = 0.25$. (a, b) Free turbulent plume and (c, d) porous media plume. The thick solid curves pertain to the well-mixed case where the source remains on indefinitely. The curves with circle and cross markers correspond to the time periods when the source is respectively on and off. Similar comments apply to the dashed curves, though these correspond to the approximate stratified model.

we can rewrite (2.21)-(2.24) as

$$\frac{\mathrm{d}\xi}{\mathrm{d}\tau} = \chi_1^{1/3}\sqrt{\mu}\left[1-\xi+\left(\frac{\chi_2}{\chi_1^{1/3}}\right)^{1/j}\frac{x_0}{H}\right]^j - \frac{1}{\sqrt{\mu}}\sqrt{\delta\xi+\delta|_{x=H}\frac{b}{H}}, \tag{2.37}$$

$$\frac{\mathrm{d}\delta}{\mathrm{d}\tau} = \frac{\sqrt{\mu}}{\xi}\left\{\chi_1 - \chi_1^{1/3}\delta\left[1-\xi+\left(\frac{\chi_2}{\chi_1^{1/3}}\right)^{1/j}\frac{x_0}{H}\right]^j\right\} + \frac{\delta-\delta|_{x=H}}{\sqrt{\mu}}\sqrt{\frac{\delta\xi+\delta|_{x=H}b/H}{\xi^2}}, \tag{2.38}$$

for a free turbulent plume and

$$\frac{\mathrm{d}\xi}{\mathrm{d}\tau} = \chi_1^{n}\sqrt{\mu}\left[1-\xi+\left(\frac{\chi_2}{\chi_1^{n}}\right)^{1/k}\frac{x_0}{H}\right]^k - \frac{1}{\sqrt{\mu}b/H}\left(\delta\xi+\delta|_{x=H}\frac{b}{H}\right), \tag{2.39}$$

$$\frac{\mathrm{d}\delta}{\mathrm{d}\tau} = \frac{\sqrt{\mu}}{\xi}\left\{\chi_1 - \chi_1^{n}\delta\left[1-\xi+\left(\frac{\chi_2}{\chi_1^{n}}\right)^{1/k}\frac{x_0}{H}\right]^k\right\} + \frac{\delta-\delta|_{x=H}}{\sqrt{\mu}b/H}\left(\frac{\delta\xi+\delta|_{x=H}b/H}{\xi}\right), \tag{2.40}$$

for a porous media plume where

$$\chi_1 = \frac{F_0+\Delta F}{F_0} \quad \text{and} \quad \chi_2 = \frac{Q_0+\Delta Q}{Q_0}. \tag{2.41}$$

Also, in (2.39) and (2.40), $n = 0$ and $n = 1/3$ correspond to point- and line-source porous media plumes, respectively.

Figure 2.9 shows the effect of changing the source volume flux of point-source free turbulent and porous media plumes with $\mu = 5$, $x_0/H = 0.1$, and $b/H = 0.1$. In both cases, the lower layer reduced gravity decreases (increases) for an increase (decrease) in the source

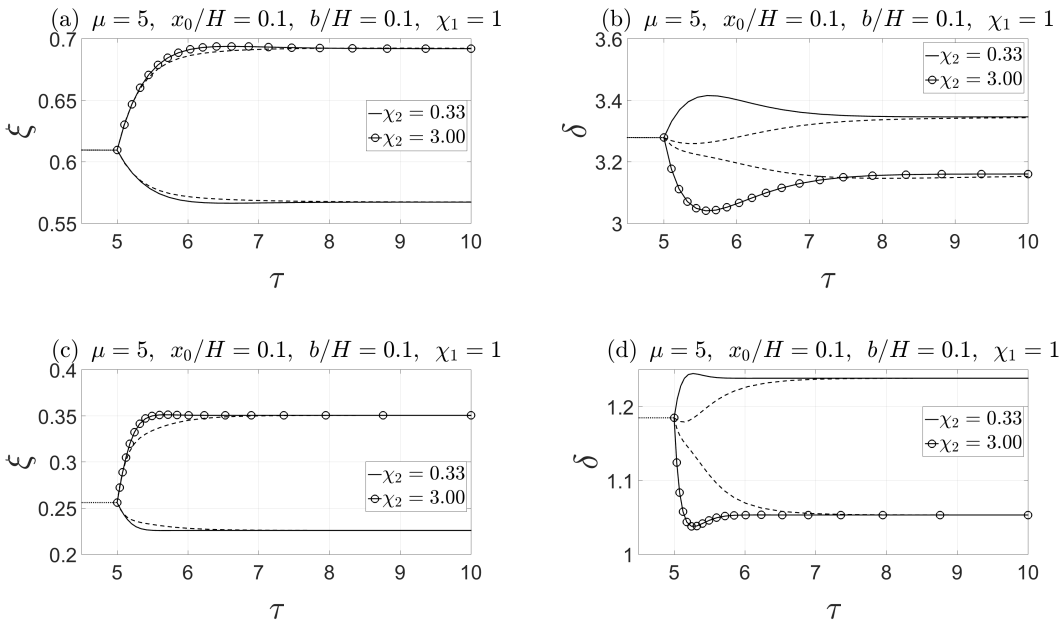

Figure 2.9: Effects of changing the source volume flux of point-source free turbulent and porous media plumes with $\mu = 10$, $b/H = 0.1$ and an initial value of x_0/H given by 0.1. (a, b) Free turbulent plume and (c, d) porous media plume. The dotted curves show the initial evolution of the system toward steady state before changing the source volume flux at $\tau = 5$. Also, the dashed curves show model predictions corresponding to the approximate stratified model.

volume flux. As a result, the outflow volume flux becomes smaller (larger) and the contaminated layer depth increases (decreases) to compensate. It should be emphasized that, for both categories of plume, the steady state depth of the contaminated layer depends on the source volume flux. Therefore changing the source volume flux results in a permanent change in the steady state value of ξ (and, of course, δ).

Figure 2.10 illustrates the effect of changing the source buoyancy flux of an ideal point-source free turbulent plume, and ideal point- and line-source porous media plumes with $\mu = 10$ and $b/H = 0.1$.

In the case of a free turbulent plume, an increase (decrease) in the source buoyancy flux results in a transient increase (decrease) in the depth of the contaminated layer. However, as the outflow from the contaminated layer adjusts, so too does ξ; ultimately the interface depth returns to its previous value. Qualitatively different behavior is seen for the case of porous media plumes. Unlike the free turbulent plume case where the steady-state depth of the contaminated layer is independent of the source buoyancy flux, the new value for ξ_{ss} is now different from the value observed before adjusting F_0. For the case of line-source porous media plumes, increasing (decreasing) the source buoyancy flux increases (decreases) the plume volume flux. Thus, the depth of the contaminated layer initially rises (falls). Correspondingly, the outflow volume flux increases (decreases) and ultimately balances the plume volume flux at a new ambient interface elevation, which is lower (higher) than its original value. However, for the case of point-source porous media plumes, (2.6) shows that the plume volume flux is, surprisingly, independent of the source buoyancy flux. Therefore, an increase (decrease) in the source buoyancy flux does not result in an initial transient increase (decrease) in the contaminated layer depth. Rather, the variation of ξ with τ is monotonic as is confirmed by figure 2.10c.

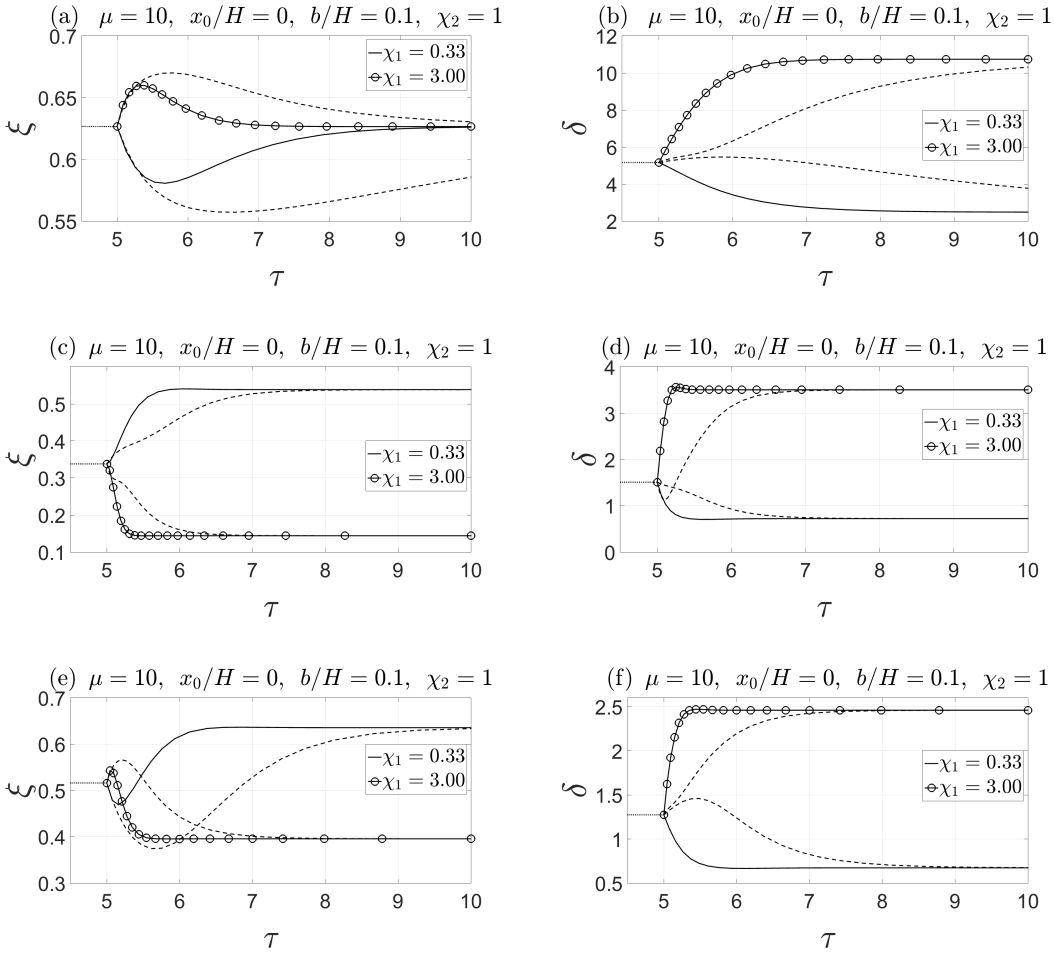

Figure 2.10: Effects of changing the source buoyancy flux of ideal point-source free turbulent, and ideal point- and line-source porous media plumes with $\mu = 10$ and $b/H = 0.1$. (a, b) Free turbulent plume, (c, d) point-source porous media plume and (e, f) line-source porous media plume. The dotted curves show the initial evolution of the system toward steady state values before changing the source buoyancy flux at $\tau = 5$. Also, the dashed curves show model predictions corresponding to the approximate stratified model.

2.6 Comparison of point- and line-source plumes in boxes filled with and devoid of porous media

In this section, we more directly compare the characteristics of flows in emptying filling boxes filled with and devoid of porous media. Because changing x_0/H and b/H does not change the dynamical features of the system except for an increase or a decrease in the contaminated layer depth and reduced gravity, we mostly consider ideal plumes with fixed lower opening depth.

Figure 2.11 illustrates, for fixed x_0/H and b/H, the variation of the depth and reduced gravity of the contaminated layer as a function of μ. As expected, and for both types of plume, ξ_{ss} increases from close to zero for small μ, to close to unity for large μ. Also, and for both plume geometries (i.e. point- and line-source), the contaminated layer depth and reduced gravity is greater in case of a free turbulent plume vs. a porous media plume.

Figure 2.12 shows the magnitude of the overshoot relative to the steady state depth. For small values of μ this relative magnitude is greater for free turbulent plumes which suggests a higher stratification in the contaminated layer. However, as μ increases, the relative magnitude of the overshoot becomes greater in the porous media plume case. Moreover, the relative magnitude of the overshoot is more significant for the approximate stratified model as compared to the well-mixed model. As μ increases however, the contaminated layer becomes nearly well-mixed and there is no distinguishable dif-

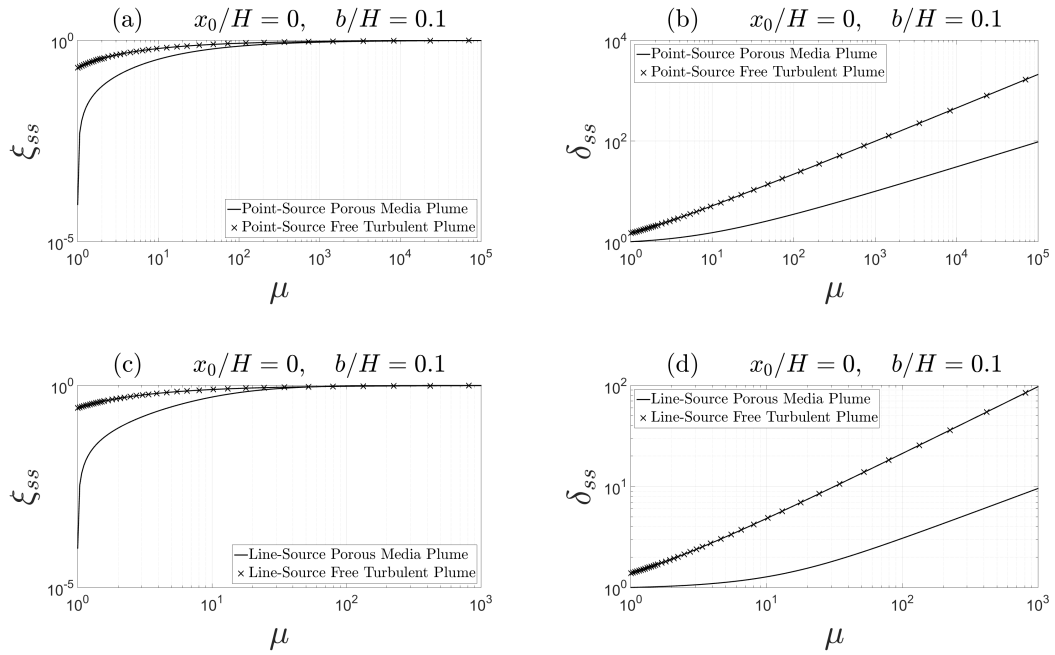

Figure 2.11: ξ_{ss} and δ_{ss} as functions of μ for ideal free turbulent and porous media plumes with $\frac{b}{H} = 0.1$. (a, b) Point-source plumes and (c, d) line-source plumes.

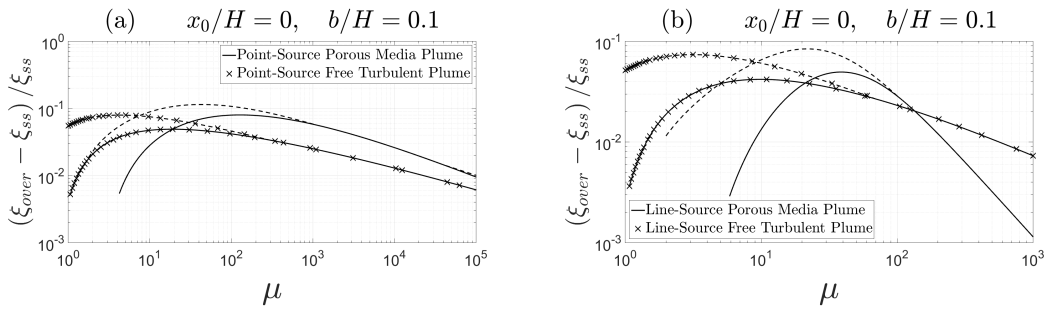

Figure 2.12: Normalized overshoot magnitude as a function of μ for ideal plumes with $\frac{b}{H} = 0.1$. (a) Point-source plumes and (b) line-source plumes. The solid and dashed curves correspond to the well-mixed and approximate stratified models, respectively.

ference between the well-mixed and approximate stratified model predictions.We noted above that the latter model anticipates overshoot for all physically-acceptable μ and also that μ_c, defined by the solution of (2.36), is relatively small for ideal plumes. In spite of this latter fact, figure 2.12 does not show results for small μ, particularly in the porous media case. This discrepancy is due to the fact that in order to correctly identify an overshoot and to define the time corresponding to it, a non-dimensional threshold value of 10^{-3} is applied. Because the overshoot amplitude falls below this threshold for relatively small μ, the overshoot is neither identified nor represented in figure 2.12 when μ is small.

Figure 2.13 shows the time, $\tau_{ss,wm}$, taken to reach 99.9% of the steady state depth for the well-mixed model. (Results corresponding to the approximate stratified model are, except for a justifiable time offset, similar and are therefore not presented here.) Initially $\tau_{ss,wm}$ increases with μ. However, for large μ, the time rate of in-

crease of the contaminated layer depth substantially increases and the lower layer spans almost the entire box. The filling of this deep contaminated layer occurs so quickly that $\tau_{ss,wm}$ later decreases with μ. The dashed lines of figure 2.13 indicate, for those cases characterized by an overshoot, the time to reach ξ_{ss} for the first time. As noted above, the time rate of increase of ξ is larger for larger μ. The time taken to first reach 99.9% of the steady state depth therefore monotonically decreases. Kaye & Hunt (2004) considered turbulent plume flow in emptying filling boxes devoid of porous media and observed, for intermediate μ, a "bulge" in their predicted values for $\tau_{ss,wm}$ (see their figure 8). This bulge was due to their definition of $\tau_{ss,wm}$ in the context of overshoot. More specifically, they identified an overshoot as occurring if $\xi_{over} - \xi_{ss} > 10^{-2}$. Our threshold value is, as noted previously, smaller and we do not therefore observe a comparable bulge in figure 2.13. If, in this figure, we had considered either a less stringent threshold value or if we had considered still larger values for μ, we would observe that the overshoot eventually becomes imperceptible. At this point, $\tau_{ss,wm}$ would decrease significantly, and the solid and dashed curves of figure 2.13 would converge. Figure 2.14 illustrates the time, τ_{over}, taken to reach the maximum overshoot depth for both the well-mixed and approximate stratified models. Similar to τ_{ss}, τ_{over} is greater in case of free turbulent plumes compared to porous media plumes.

For the case of an ideal source that is turned on and off with half-period $\Delta\tau$, figure 2.15 compares the aforementioned extrema of ξ and δ for the two plume configurations. If $\Delta\tau$ is large enough,

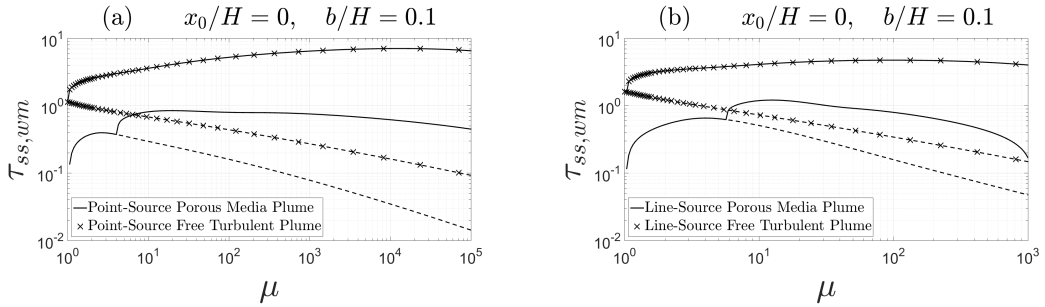

Figure 2.13: $\tau_{ss,wm}$ as a function of μ for ideal plumes with $\frac{b}{H} = 0.1$. (a) Point-source plumes and (b) line-source plumes. The solid and dashed curves correspond, respectively, to the time needed to reach 99.9% of the steady state depth and, for those cases having an identifiable overshoot, the initial time to reach this same elevation.

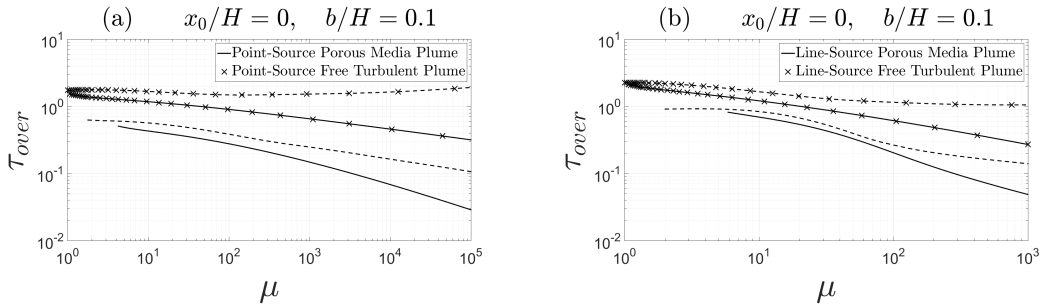

Figure 2.14: Time taken to reach the maximum overshoot depth as a function of μ for ideal plumes with $\frac{b}{H} = 0.1$. (a) Point-source plumes and (b) line-source plumes. The solid and dashed curves correspond to the well-mixed and approximate stratified models, respectively.

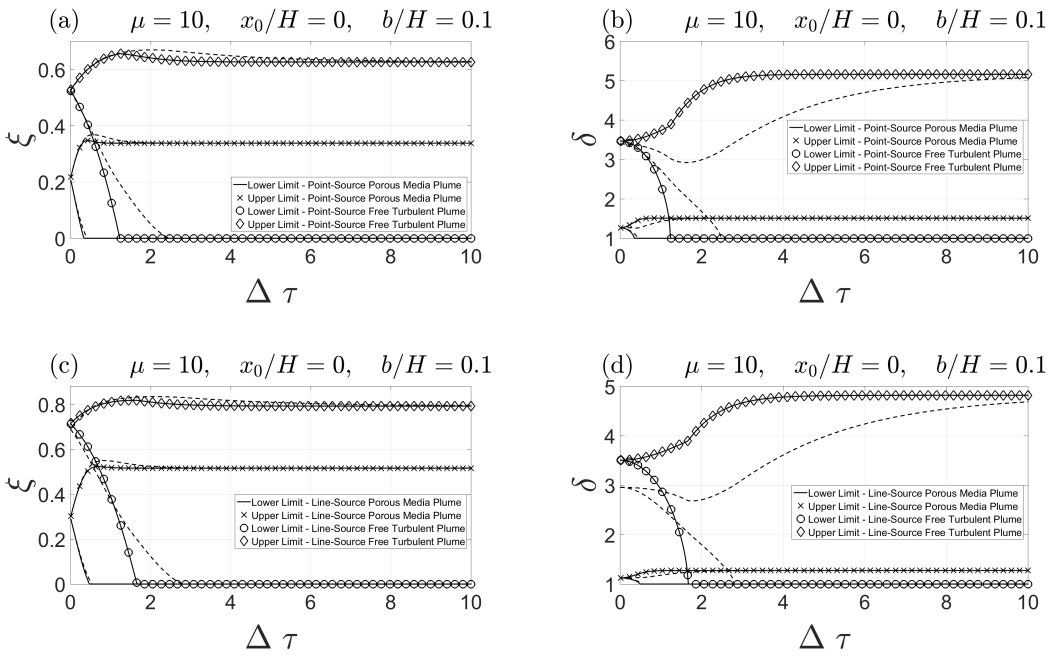

Figure 2.15: Extrema of ξ and δ after a number of cycles for ideal free turbulent and porous media plumes. (a, b) Point-source plumes and (c, d) line-source plumes. The solid and dashed curves correspond to the well-mixed and approximate stratified models, respectively.

all of the contaminated fluid drains from the bottom of the box, which is then comprised of uniform ambient fluid, represented on figures 2.15b and 2.15d by $\delta = 1$. Similar to the previous results and for prescribed μ, x_0/H and b/H, the extrema of both ξ and δ are greater for free turbulent plumes than for porous media plumes, often significantly so.

Figure 2.16 shows the steady state depth and reduced gravity of the contaminated layer after changing the source volume flux while keeping the source buoyancy flux constant. From section 2.5, we know that increasing (decreasing) the source volume flux results in an increase (a decrease) in the steady state depth of the contami-

nated layer. Figure 2.17 illustrates the time taken to reach 99.9% of the steady state depth after changing the source volume flux for both the well-mixed and approximate stratified models. Depending on the magnitude of χ_2, the contaminated layer depth may undershoot or overshoot its steady state value. Again we apply a criterion where the difference between the magnitude of the maximum overshoot/undershoot and the steady state depth after changing Q_0 must be greater than 10^{-3}. Otherwise, we do not consider an overshoot/undershoot to have occurred. There is in figure 2.17 therefore a pair of sudden jumps in $\Delta\tau$ that are observed for the free turbulent plume case. For instance, in figure 2.17a, such sudden jumps are observed when $\chi_2 \simeq 0.25$ and $\chi_2 \simeq 1.95$ for a point-source free turbulent plume with the well-mixed model. No such sudden jumps are noted in the analogue porous media case because, within the accuracy imposed by our threshold, no overshoot/undershoot occurs. It should be noted that in figure 2.17, the gap near $\chi_2 = 1$ is due to the fact that in order to accurately measure a departure from the original steady state, we used the criterion that the difference between the new and old values for ξ_{ss} had to exceed 10^{-3}.

Figure 2.18 shows the steady state depth and reduced gravity of the contaminated layer after changing the source buoyancy flux while keeping the source volume flux constant. In the case of free turbulent plumes, μ is independent of the source buoyancy flux (see equation 2.25). Hence, changing F_0 does not alter the contaminated layer steady state depth for either source geometry. However, μ is a function F_0 in case of porous media plumes and a change in F_0 therefore results in a corresponding increase or decrease in ξ_{ss}. Be-

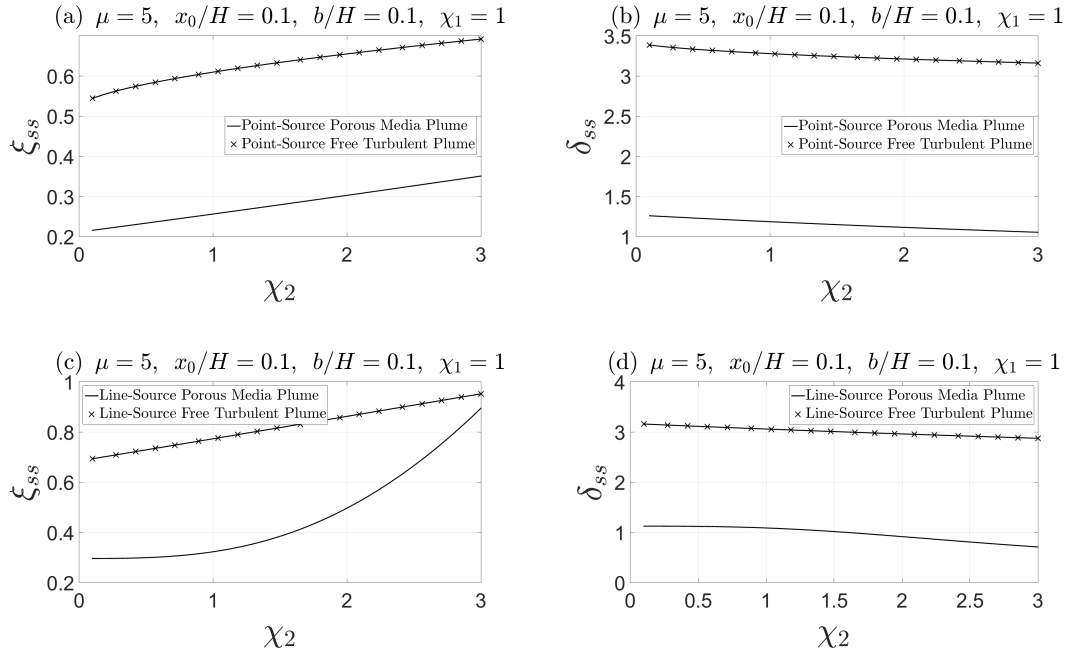

Figure 2.16: Steady state depth and reduced gravity of the contaminated layer after changing the source volume flux of free turbulent and porous media plumes. (a, b) Point-source plumes and (c, d) line-source plumes.

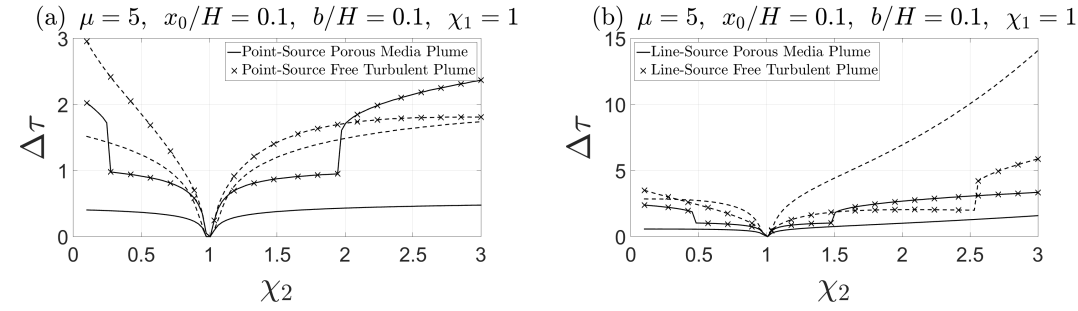

Figure 2.17: Time taken to reach 99.9% of the steady state depth after changing the source volume flux of free turbulent and porous media plumes. (a) Point-source plumes and (b) line-source plumes. The solid and dashed curves correspond to the well-mixed and approximate stratified models, respectively.

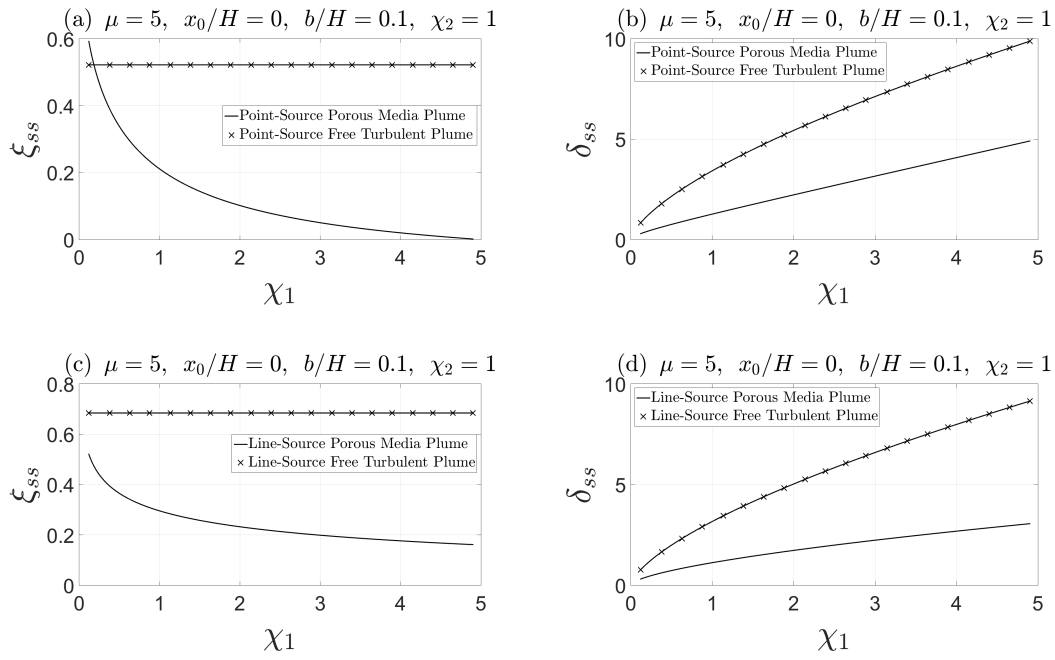

Figure 2.18: Contaminated layer steady state depth and reduced gravity after changing the source buoyancy flux of free turbulent and porous media plumes. (a, b) Point-source plumes and (c, d) line-source plumes.

cause we imagine a fixed source volume flux, changes to the source buoyancy flux are synonymous with changes to the source reduced gravity. Hence, as χ_1 increases or decreases, so too does the contaminated layer reduced gravity. Figure 2.19 depicts the time taken to reach 99.9% of the steady state depth after changing the source buoyancy flux for both the well-mixed and approximate stratified models. As expected, it takes longer to approach steady state according to the approximate stratified model for both free turbulent and porous media plumes. Also, the porous media plumes reach steady conditions faster than the free turbulent plumes.

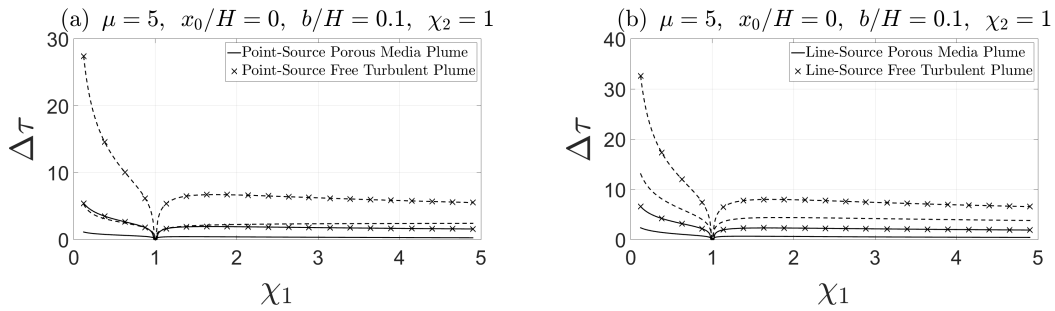

Figure 2.19: Time taken to reach 99.9% of the steady state depth after changing the source buoyancy flux of free turbulent and porous media plumes. (a) Point-source plumes and (b) line-source plumes. The solid and dashed curves correspond to the well-mixed and approximate stratified models, respectively.

2.7 Conclusions

The principal contribution of this study is to outline a mathematical methodology by which the emptying filling box behavior of a control volume filled with porous media may be approximated. Specific reference is made to two end member cases, namely one where the contaminated layer is assumed to be uniform and another where the density of the discharged fluid is supposed to equal the plume density at the level of the interface. The predictions associated with these models typically represent upper and lower bounds; the bounds become increasingly sharp in the limit of large μ where μ is defined by the ratio of the draining timescale to the filling timescale. This ratio plays an equally critical role in the analogue and well-studied problem of an emptying filling box devoid of porous media. Indeed, the governing equations (2.21-2.22) appropriate to this free turbulent plume case closely resemble those germane to a laminar porous media plume (2.23-2.24). Our solution of these judiciously

non-dimensionalized equations confirms that comparable dynamical behaviour is often observed notwithstanding the important physical differences between laminar and turbulent plumes. For instance, we have demonstrated that for a box filled initially with ambient fluid, the contaminated layer depth may overshoot its steady state value. Furthermore, while the well-mixed model will only predict an overshoot if μ exceeds a threshold value, μ_c, no such limitation applies to the approximate stratified model, which admits overshoot for small and large μ alike.

Our study has also considered time-varying conditions where the buoyancy source is either turned on and off with a half-period of $\Delta\tau$ or subjected to a limited increase or decrease in the source buoyancy flux or volume flux. We showed that when the source is turned on and off periodically, the depth and reduced gravity of the contaminated layer oscillates between two extrema after a handful of cycles. In the case of an increase (decrease) in the source volume flux, Q_0, the reduced gravity of the contaminated layer decreases (increases) which results in a permanent increase (decrease) in the contaminated layer depth. Different behaviour is noted when adjusting the source buoyancy flux, F_0, at least when considering boxes devoid of porous media. The contaminated layer depth is then independent of F_0 and so the original depth is recovered after some transient adjustment phase. On the other hand, the steady state depth of the contaminated layer is a function of F_0 for porous media plumes; thus, a change in the source buoyancy flux leads to a permanent change of interface depth, analogous to the case where

Q_0 is altered.

Chapter 3

Conclusions

In this study, we have investigated the transient dynamics of emptying filling box flows in boxes filled with a porous medium. For the analogue problem involving turbulent plumes and boxes devoid of porous media, an exact solution can be obtained by using an algorithm due to Germeles (1975). Unfortunately, no such algorithm is available for porous media plumes. On the other hand, it is possible to bracket the exact solution (for sufficiently large time, t) by considering two bookend opposite scenarios. In the former, the lower contaminated layer is assumed to be well-mixed. In the latter, the contaminated layer is assumed to be stratified with a density along the bottom boundary that is equal to the plume density at the elevation of the first front, the interface separating contaminated from uncontaminated ambient fluid. We have also shown that the range of possible solutions becomes narrow as μ increases, where μ is the ratio of the draining timescale to the filling timescale. Our technique is justified by drawing numerous comparisons between the free turbulent and porous media plume cases. Moreover, we demonstrate that while free turbulent and porous media plumes are two distinct

physical phenomena, the non-dimensional governing equations and, in some cases, the dynamical behaviours are quite similar.

In this study, we consider three different scenarios, namely cases where the initial interior density equals the density of the infinite ambient external to the filling box, other cases where the plume source is sequentially turned on and off with a half-period of $\Delta\tau$, and still other cases where the plume source is subjected to a limited increase or decrease of the source buoyancy flux or volume flux. We showed that when the box is initially filled with uncontaminated ambient fluid, the contaminated layer may overshoot its steady state depth. While such an overshoot is anticipated by the approximate stratified model for all μ, the overshoot appears in the well-mixed model only for μ larger than a critical value. For the case of a cyclic source, we demonstrated that, after a few cycles, the depth and reduced gravity of the contaminated layer oscillates between two extrema whose values depend on μ, x_0/H, and b/H. When the source volume flux is changed, the behavior is qualitatively similar to the free turbulent media plume case. There is, in other words, a permanent change in the depth, ξ, and reduced gravity, δ, of the contaminated layer where ξ and δ respectively increase and decrease with increasing source volume flux. Finally, for the case of an increase or a decrease in the source buoyancy flux, we observe different behaviour between the free turbulent and porous media plume cases. For free turbulent plumes, the steady state depth of the contaminated layer is independent of the source buoyancy flux. As a result, a change in F_0 results only in a transient adjustment

of the interface depth, where after it relaxes to its original steady state value. Much different behavior is noted in the case of porous media plumes. Here, the steady state depth of the contaminated layer does depend on F_0 and therefore an increase (decrease) in F_0 results in a permanent decrease (increase) in ξ.

Having gained a better understanding of the transient dynamics of emptying filling box flows in boxes filled with porous media, there remain numerous areas for subsequent investigation. Specific topics for future studies are identified as:

- In this study, we have considered Boussinesq, Darcy flows with miscible fluids. While non-Darcy flows can be modeled through the introduction of Dupuit-Forchheimer terms to the governing equations, the Boussinesq and miscibility assumptions depend on the nature of the problem and the chemical composition of the fluids in question. For instance, in carbon sequestration, the supercritical CO_2 and brine exhibit only a very limited miscibility of one phase into the other. Relaxing any of the above assumptions can further our knowledge towards more practical situations.

- We have further assumed that the dispersion coefficient is spatially-invariant and is equal to the molecular diffusion coefficient. However, when the Péclet number, defined as the ratio of the advective transport rate to the diffusive transport rate, is large, the effects of mechanical dispersion should also be considered. Sahu & Flynn (2015, 2016*b*) derived expressions for the plume

volume flux under the assumption that Pe $\gtrsim \mathcal{O}(1)$, which can be used instead of (2.6) and (2.7). Making such a change is expected to be qualitatively inconsequential in some contexts, but quite significant in others. Consider, for instance, the response to a change of source buoyancy flux, F_0, in case of a plume emanating from a point source. According to the current formulation, such a change of F_0 results in a monotonic change in the contaminated layer depth because, the plume volume flux, Q_p, is independent of the source buoyancy flux. However, according to Sahu & Flynn (2016*b*), Q_p depends on F_0 for Pe $\gtrsim \mathcal{O}(1)$. Therefore, if Sahu & Flynn (2016*b*) expression is used, we would observe non-monotonic behaviour similar to that of a line-source porous media plume (figure 2.10e).

- In real geophysical problems such as those mentioned in Chapter 1, the permeability and porosity of both the box and the fissure(s) may be highly non-uniform. Hence, it is necessary to revisit the Darcy equations (equations (2.2) and (2.3) of Roes *et al.*, 2014) in order to account for such non-uniformities. Although, an analytical solution may not be easily obtained, numerical modeling could be used to solve the modified governing equations.

Bibliography

Adalsteinsson, D., Camassa, R., Harenberg, S., Lin, Z., Mclaughlin, R. M., Mertens, K., Reis, J., Schlieper, W. & White, B. 2011 Subsurface trapping of oil plumes in stratification: laboratory investigations. *Monitoring and Modeling the Deepwater Horizon Oil Spill: A Record-Breaking Enterprise* pp. 257–262.

Baines, W. D. 1983 Direct measurement of volume flux of a plume. *J. Fluid Mech.* **132**, 247–256.

Baines, W. D. & Turner, J. S. 1969 Turbulent buoyant convection from a source in a confined region. *J. Fluid Mech.* **37**, 51–80.

Bickle, M. J. 2009 Geological carbon storage. *Nature Geoscience* **2**, 815–818.

Bolster, D. 2014 The fluid mechanics of dissolution trapping in geologic storage of co_2. *J. Fluid Mech.* **740**, 1–4.

Bolster, D. T. & Caulfield, C. P. 2008 Transients in natural ventilationa time-periodically-varying source. *Build. Ser. Engng Res. Technol.* **29** (2), 119–135.

Bolster, D. T., Maillard, A. & Linden, P. F. 2008 The response of natural displacement ventilation to time-varying heat sources. *Energy and Buildings* **40** (12), 2099–2110.

Boyce, W.E. & DiPrima, R.C. 2008 *Elementary Differential Equations and Boundary Value Problems*. Wiley.

Bush, J. & Woods, A. W. 1999 Vortex generation by line plumes in a rotating stratified fluid. *J. Fluid Mech.* **388**, 289–313.

Caulfield, C. P. & Woods, A. W. 2002 The mixing in a room by a localized finite-mass-flux source of buoyancy. *J. Fluid Mech.* **471**, 33–50.

Dentz, M. & Tartakovsky, D. M. 2009 Abrupt-interface solution for carbon dioxide injection into porous media. *Trans. Porous Med.* **79** (1), 15–27.

Flynn, M. R. & Caulfield, C. P. 2006 Natural ventilation in interconnected chambers. *J. Fluid Mech.* **564**, 139–158.

Germeles, A. E. 1975 Forced plumes and mixing of liquids in tanks. *J. Fluid Mech* **71**, 601–623.

Holford, J. M. & Hunt, G. R. 2000 Multiple steady states in natural ventilation. In *Proc. 5th Intl. Symp. on Stratified Flows, Vancouver* (ed. G. A. Lawrence, R. Pieters & N. Yonomitsu), pp. 661–666.

Kaye, N. B., Flynn, M. R., Cook, M. J. & Ji, Y. 2010 The role of diffusion on the interface thickness in a ventilated filling box. *J. Fluid Mech.* **652**, 195–205.

Kaye, N. B. & Hunt, G. R. 2004 Time-dependent flows in an emptying filling box. *J. Fluid Mech.* **520**, 135–156.

Kaye, N. B. & Hunt, G. R. 2007 Smoke filling time for a room due to a small fire: the effect of ceiling height to floor width aspect ratio. *Fire Safety Journal* **42** (5), 329–339.

Kaye, N. B., Ji, Y. & Cook, M. J. 2009 Numerical simulation of transient flow development in a naturally ventilated room. *Building and Environment* **44** (5), 889–897.

Kneafsey, T. J. & Pruess, K. 2010 Laboratory flow experiments for visualizing carbon dioxide-induced, density-driven brine convection. *Trans. Porous Med.* **82** (1), 123–139.

Kueper, B. H., Wealthall, G. P., Smith, J. W. N., Leharne, S. A. & Lerner, D. N. 2003 An illustrated handbook of dnapl transport and fate in the subsurface. *Tech. Rep.* R&D Publication 133. Environment Agency.

Lin, Y. J. P. & Linden, P. F. 2002 Buoyancy-driven ventilation between two chambers. *J. Fluid Mech.* **463**, 293–312.

Linden, P. F. 1999 The fluid mechanics of natural ventilation. *Ann. Rev. Fluid Mech.* **31** (1), 201–238.

Linden, P. F., Lane-Serff, G. F. & Smeed, D. A. 1990 Emptying filling boxes: the fluid mechanics of natural ventilation. *J. Fluid Mech.* **212**, 309–335.

MacKay, D. J. 2009 *Sustainable energy – without the hot air*. UIT Cambridge Ltd.

May, D. 2009 *Fluid Flow*. Douglass H. May.

McDougall, T. J. 1978 Bubble plumes in stratified environments. *J. Fluid Mech.* **85** (04), 655–672.

Morton, B. R., Taylor, G. I. & Turner, J. S. 1956 Turbulent gravitational convection from maintained and instantaneous sources. *Proceedings of the Royal Society of London A: Mathematical, Physical and Engineering Sciences* **234** (1196), 1–23.

Nabi, S. & Flynn, M. R. 2013 The hydraulics of exchange flow between adjacent confined building zones. *Building and Environment* **59**, 76–90.

Riaz, A., Hesse, M., Tchelepi, H. A. & Orr, F. M. 2006 Onset of convection in a gravitationally unstable diffusive boundary layer in porous media. *J. Fluid Mech.* **548** (1), 87–111.

Roes, M. A., Bolster, D. T. & Flynn, M. R. 2014 Buoyant convection from a discrete source in a leaky porous medium. *J. Fluid Mech.* **755**, 204–229.

Sahu, C. K. & Flynn, M. R. 2015 Filling box flows in porous media. *J. Fluid Mech.* **782**, 455–478.

Sahu, C. K. & Flynn, M. R. 2016*a* The effect of sudden permeability changes in porous media filling box flows. *under review with J. Fluid Mech.* .

Sahu, C. K. & Flynn, M. R. 2016*b* Filling box flows in an axisymmetric porous medium. *Trans. Porous Med.* **112** (3), 619–635.

Sauty, J. P., Gringarten, A. C., Menjoz, A. & Landel, P. A. 1982 Sensible energy storage in aquifers: Theoretical study. *Water Resour. Res.* **18**, 245–252.

Speer, K. G. & Marshall, J. 1995 The growth of convective plumes at seafloor hot springs. *J. Marine Res.* **53** (6), 1025–1057.

Speer, K. G. & Rona, P. A. 1989 A model of an atlantic and pacific hydrothermal plume. *J. Geophys. Res. Oceans* **94** (C5), 6213–6220.

Vauquelin, O. 2015 Oscillatory behaviour in an emptying–filling box. *J. Fluid Mech.* **781**, 712–726.

Wooding, R. A. 1963 Convection in a saturated porous medium at large rayleigh number or peclet number. *J. Fluid Mech.* **15** (04), 527–544.

Woods, A. W. 1988 The fluid dynamics and thermodynamics of eruption columns. *Bull. Volcanol.* **50** (3), 169–193.

Woods, A. W. 2010 Turbulent plumes in nature. *Ann. Rev. Fluid Mech.* **42**, 391–412.

Worster, M. G. & Huppert, H. E. 1983 Time-dependent density profiles in a filling box. *J. Fluid Mech.* **132**, 457–466.

Wüest, A., Brooks, N. H. & Imboden, D. M. 1992 Bubble plume modeling for lake restoration. *Water Resour. Res.* **28** (12), 3235–3250.

Appendices

Appendix A

A brief description of the Germeles algorithm

In this study, a modified version of the Germeles (1975) algorithm is employed to find the exact solution for an emptying filling box devoid of porous media and containing a free turbulent plume. Because Germeles's algorithm relies on the analysis of Baines & Turner (1969), which is itself a nontrivial extension of Morton *et al.* (1956), it is beneficial to review some of the salient details of turbulent plume theory before turning to the numerical aspects. In this spirit, recall that Morton *et al.* (1956) considered an axisymmetric point source and Boussinesq fluids. Their model is based on the evolution of the plume volume flux, Q_p, momentum flux, M_p, and buoyancy flux F_p, which, for top-hat variables, respectively satisfy the following ordinary differential equations:

$$\frac{\mathrm{d}Q_p}{\mathrm{d}x} = 2\alpha_p\sqrt{\pi M_p}, \tag{A.1}$$

$$\frac{\mathrm{d}M_p}{\mathrm{d}x} = \frac{Q_p F_p}{M_p}, \tag{A.2}$$

$$\frac{\mathrm{d}F_p}{\mathrm{d}x} = -Q_p\frac{\partial g'}{\partial x}, \tag{A.3}$$

where the parameter $\alpha_p \simeq 0.117$ is the entrainment coefficient and is equal to the ratio of the entrainment velocity to the plume vertical velocity. Following Baines & Turner (1969), we assume that the flow is of a sufficiently large scale so that advection is dominant compared to diffusion. As the plume reaches the bottom boundary, it forms a thin layer of discharged fluid which is, in turn, re-entrained into the plume so that the next layer of discharged fluid is slightly more dense than that which was deposited just before. Thus, the above equations must be supplemented by a conservation of mass equation valid for the lower layer of the ambient, which can be written as

$$\frac{\partial g'}{\partial t} + u\frac{\partial g'}{\partial x} = 0, \tag{A.4}$$

where u is the upward advection velocity outside the plume. This advection or return flow velocity can easily be determined if we assume that the cross-section of the plume is small compared to the cross-section of the box. Thus, the entrainment into the plume is horizontal. Assuming that the box aspect ratio is small, the return flow velocity can be found by means of volume conservation:

$$uS = Q_p - Q_{out}, \tag{A.5}$$

where Q_{out} is the volumetric rate of outflow through the lower opening defined in (2.5). Now, we introduce the following non-

dimensional variables:

$$q = \frac{Q_p}{CH^{5/3}F_0^{1/3}}, \tag{A.6}$$

$$m = \frac{4\alpha^2\pi}{C^2H^{4/3}F_0^{2/3}}M_p, \tag{A.7}$$

$$f = \frac{F_p}{F_0}, \tag{A.8}$$

$$\delta = \frac{CH^{5/3}}{F_0^{2/3}}g', \tag{A.9}$$

where q, m and f respectively represent non-dimensional plume volume, momentum, and buoyancy fluxes, and δ is the non-dimensional reduced gravity of the contaminated layer. Subsequently (A.1)-(A.4) can be non-dimensionalized as follows:

$$\frac{\mathrm{d}q}{\mathrm{d}\xi} = \sqrt{m}, \tag{A.10}$$

$$\frac{\mathrm{d}m}{\mathrm{d}\xi} = \beta\frac{qf}{m}, \tag{A.11}$$

$$\frac{\mathrm{d}f}{\mathrm{d}\xi} = -q\frac{\partial\delta}{\partial\xi}, \tag{A.12}$$

$$\frac{\partial\delta}{\partial\tau} = \sqrt{\mu}\,(q - q_{out})\,\frac{\partial\delta}{\partial\xi}, \tag{A.13}$$

in which $\beta = 5^4/3^5$ and μ is the ratio of the draining to the filling timescales defined in (2.25).

In Germeles's algorithm, the ambient is discretized into a finite number of layers. Also, the density of the ambient is assumed to evolve very slowly compared to the plume. Thus, and from the point of view of plume rise, the ambient density stratification can be considered as quasi-static. Consequently, the plume volume and momentum flux equations (A.10-A.11) may at every time step and

for prescribed boundary conditions be solved assuming a frozen ambient density field. Note that for an ideal source the boundary conditions are trivial, at least with respect to q and m, i.e.

$$q = m = 0 \quad \text{and} \quad f = 1 \quad \text{at} \quad \xi = 0 \quad \text{for} \quad \tau \geq 0. \tag{A.14}$$

Since the profile of δ is known at time τ, integration of (A.12) with the boundary condition for f yields

$$f(i+1) = f(i) - q(i+1)\left[\delta(i+1) - \delta(i)\right], \quad 1 \leq i < n. \tag{A.15}$$

The density layers are then advected upward with a velocity calculated using the discretized version of (A.5). Reverting to dimensional variables, we write

$$u(i)S = Q_p(i) - Q_{out}. \tag{A.16}$$

In (A.15) and (A.16), the index i is a label for each density layer $(1 < i < n)$. Each layer is then advected upwards as

$$x_{new}(i) = x_{old}(i) + u(i)\Delta t, \tag{A.17}$$

which can be written in non-dimensional form as

$$\xi_{new}(i) = \xi_{old}(i) - \sqrt{\mu}\left[q(i) - q_{out}\right]\Delta\tau. \tag{A.18}$$

Of course, each time step is associated not only with the advection of existing layers of the contaminated fluid, but also with the creation of two new layers: one at the bottom of the box from fluid discharged by the plume and one at the top of the box from the inflow of the ambient fluid. The new ambient fluid layer has a depth of

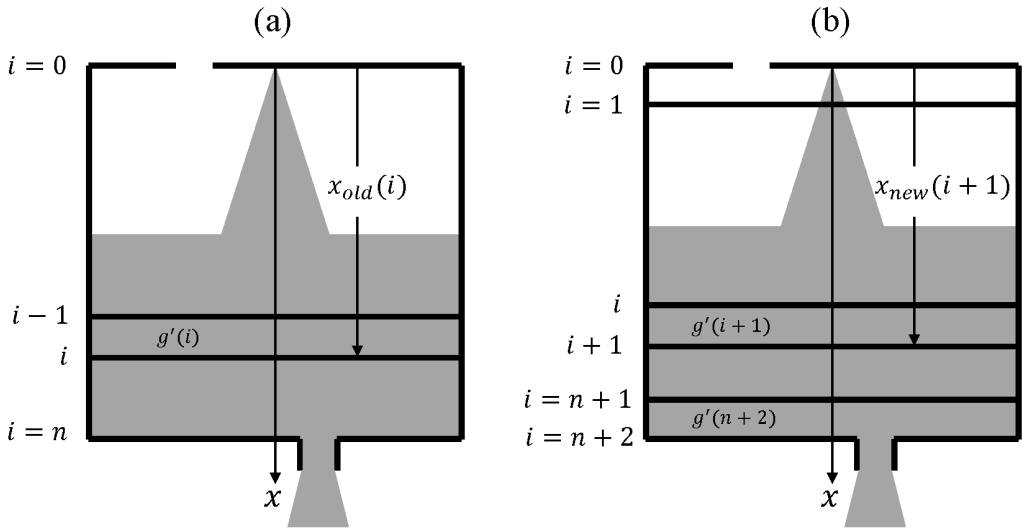

Figure A.1: Schematic illustrating Germeles's numerical scheme at times (a) t and (b) $t + \Delta t$. Over the time interval Δt, the layer comprised of fluid with reduced gravity $g'(i)$ is advected upward from $x_{old}(i)$ to $x_{new}(i+1)$ according to (A.17). The change of index from i to $i+1$ is necessitated by the introduction of a new ambient layer just below the source.

$Q_{out}\Delta t$ which can be non-dimensionalized as $1/\sqrt{\mu}\sqrt{\int_0^1 \delta \mathrm{d}\xi}\Delta\tau$. The depth and reduced gravity of the new contaminated fluid layer at the bottom of the box may also be written in terms of the plume properties via

$$\xi(n+2) = 1 - \sqrt{\mu}\left[q(i) - q_{out}\right]\Delta\tau, \tag{A.19}$$

$$\delta(n+2) = \delta(n) + \frac{f(n)}{q(n)}. \tag{A.20}$$

Moreover, due to entrainment, the layers get progressively thinner. Once the layer thickness falls below a critical value, a merging operation is performed with the adjacent layer so that the local average value of δ is preserved.

Appendix B

The Germeles algorithm – MATLAB code

In this appendix, an algorithm is presented and described that solves (A.10)-(A.13). A brief description and list of input/output variables for each of the MATLAB programs highlighted below is presented in table B.1. Furthermore, the evolution of the contaminated layer depth for different values of the time-step sizes is considered in figure B.1, which shows that a step size of 0.025 provides a sufficiently accurate results.

Table B.1: Description and list of input/output variables for each of the MATLAB programs highlighted below.

File Name	Inputs/Outputs	Description
germ.m	inputs: μ and τ_{max}. outputs: ξ, δ, $\delta\|_{x=H}$ and $\delta\|_{x=H-h}$.	This script is the "master" program; it implements the Germeles (1975) algorithm for a negatively-buoyant ideal plume and plots the non-dimensional depth and reduced gravity of the contaminated layer as well as the non-dimensional reduced gravities at the bottom of the box and at the interface height.
vertprof.m	None	This script computes the vertical profiles of q, m and f at the given non-dimensional time, τ. The ordinary differential equations are solved using `MATLAB`'s built-in `ode45` function
qm.m	inputs: q and m. outputs: $\mathrm{d}q/\mathrm{d}\zeta$ and $\mathrm{d}m/\mathrm{d}\zeta$	This function calculates the vertical derivatives of q and m at the given non-dimensional time, τ.
zzdelta.m	None	This scripts computes, at the new time step, the depths and densities of the different layers comprising the discharged plume fluid layer.

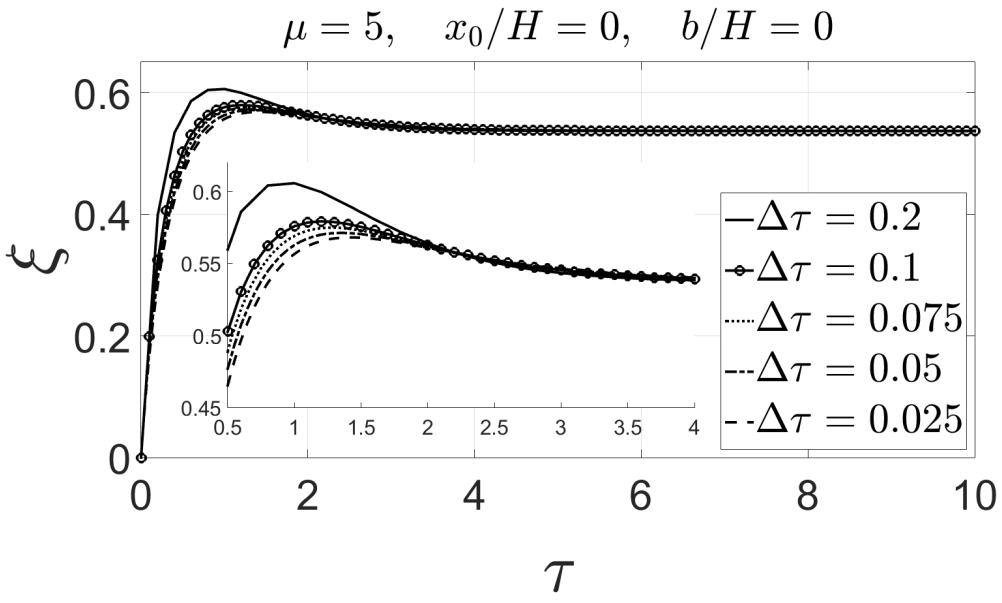

Figure B.1: Evolution of the contaminated layer depth for different time-step sizes.

```
% This script implements the routine of Germeles (1975)
   for a negatively-buoyant ideal plume.

global ff mu mu taumax

% Define variables.
mu=10;
EPS=1e-6;
Steptol=1e-4; %The criterion for the layers to be absorbed
    by the adjacent layers.
step=50;        % Initial number of vertical levels. Note
   that an extra level is added at each iteration.
ximin=-1.0; % ximax is assumed to be 0, i.e. the plume
   source sits at xi=0.
deltamin=0.0; % deltamin and deltamax determine the
   initial stratification in the ambient.
deltamax=0.0;
tau=0.0;
Deltatau=0.025; % Set the non-dimensional time increment.

% Initialize arrays.
zz=zeros(1,step+1);
delta=zeros(1,step);

% Set values of arrays zz and delta.
zz=linspace(0, ximin, step+1);
delta=linspace(deltamax, deltamin, step); % delta has a `
   staircase' structure whose `granularity' is set by the
   size of step.
i_tra=1;
zz_tra(1)=0;
delta_tra(1)=0;
delta_end(1)=0;
delta_inter(1)=0;
tau_tra(1)=0;

while (tau<=taumax)
clear q m f zeta Q % Clear arrays q, m, f, zeta and Q.
 % Initialize arrays.
f=zeros(1,step); % f records the value of f within each
   step. f has a `staircase' structure much like delta.
Q=zeros(1,step+1); % Q records the value of q at zz0, zz1,
    etc.
```

```
M=zeros(1,step+1); % M records the value of m at zz0, zz1,
    etc.

 % Specify conditions at zeta=0 (i.e. the boundary
    conditions).
Q(1)=-EPS;
M(1)=EPS;
f(1)=1.0;

 % Compute the vertical profiles of q, m and f. See
    vertprof.m.
vertprof;

 % Update the arrays zz and delta. See zzdelta.m
zzdelta;

 % Calculate the average density of the contaminated layer
    .
for i=1:step
    if delta(i) < -1e-3
        i_tra=i_tra+1;
        tau_tra(i_tra)=tau;
        zz_tra(i_tra)=1-abs(zz(i));
        delta_tra(i_tra)=trapz(zz(2:end),delta/2^(2/3))/
           zz_tra(i_tra);
        delta_end(i_tra)=abs(delta(end))/2^(2/3);
        for j=1:length(f)
            if f(j) < 1
                delta_inter(i_tra)=abs(f(j-1)/Q(j))
                   /2^(2/3);
                break
            end
        end
        break;
    end
end

end
delta = delta/2^(2/3);

f1 = figure;
xlim([0 10]);
set(gca,'FontSize',48)
```

```
hold on
box on
grid on
xlabel('\tau','FontSize',80)
ylabel('\xi','FontSize',80)
f2 = figure;
xlim([0 10]);
set(gca,'FontSize',48)
box on
hold on
grid on
xlabel('\tau','FontSize',80)
ylabel('\delta','FontSize',80)

set(0, 'CurrentFigure', f1)
f_xi(1) = plot(tau_tra,zz_tra,':k','LineWidth',3.0);

set(0, 'CurrentFigure', f2)
f_gamma(1) = plot(tau_tra,delta_tra,':k','LineWidth',3.0);
f_gamma(2) = plot(tau_tra,delta_end,'LineWidth',2.0);
f_gamma(3) = plot(tau_tra(1:end-1),delta_inter(2:end),'
    LineWidth',2.0);

s{1} = 'Germeles Algorithm';
s{2} = '\delta at the bottom of the box';
s{3} = '\delta at the interface height';

set(0, 'CurrentFigure', f1)
legend(f_xi,s,'interpreter','latex','FontSize',48,'
    Location','SE')
str=['$\mbox{(a)} \qquad \mu=' num2str(mu) ',\quad \frac{
    x_0}{H}=0,\quad \frac{b}{H}=0$'];
title(str,'interpreter','latex','FontSize',48)

set(0, 'CurrentFigure', f2)
legend(f_gamma,s,'interpreter','latex','FontSize',48,'
    Location','SE')
str=['$\mbox{(b)} \qquad \mu=' num2str(mu) ',\quad \frac{
    x_0}{H}=0,\quad \frac{b}{H}=0$'];
title(str,'interpreter','latex','FontSize',48)
```

```
% vertprof.m computes the vertical profiles of q, m and f
   at the given value of tau. f1 is given from the
   boundary condition. This allows us to integrate (A.10)
   and (A.11) using the integration scheme ode45. This
   gives the values of q1 and m1 from which f2 can be
   computed from the discrete form of (A.12). Then we
   integrate to find q2 and m2, etc. all the way down to
   the bottom of the box. This cycle is repeated step
   times where step is the number of steps in the density
   profile for the particular value of tau.

for i=1:step
 % Specify ff which is known either from the BC or the
    previous iteration.
ff=f(i);

 % Determine the zeta interval of integration and the
    appropriate BCs.
xiint=[zz(i) zz(i+1)];
init=[Q(i) M(i)];

 % Solve the diff. equations for q and m.
[Zeta F]=ode45(@qm,xiint,init);

 % Update the arrays Q and M.
Q(i+1)=F(end,1);
M(i+1)=F(end,2);

if (i<step) % Compute the value of f to be used at the
   next iteration.
  f(i+1)=f(i)-Q(i+1)*(delta(i+1)-delta(i));
end

end
```

```
function dF=qm(~,F)

% qm.m solves the coupled system of odes (A.10-A.12) where
    it is assumed that f=ff is known either from the
   boundary condition or from the previous iterate.

global ff

dF=zeros(2,1);
dF(1)=sqrt(F(2));
dF(2)=5^4/3^5*ff*F(1)/F(2);
```

```
% zzdelta.m computes the updated values of zz (the
   vertical position of the isopycnal surfaces) and delta
   (the density within each step).

global mu;
tau=tau+Deltatau;
% The outflow volume flux.
q_v=1/mu*sqrt(abs(trapz(zz(2:end),delta)));
if (tau<=taumax)
% The position of the new ambient layer.
zz_new=-sqrt(mu)*q_v*Deltatau;
% Compute new position of isopycnal surfaces.
for i=1:step+1
  zz(i)=zz(i)-sqrt(mu)*(Q(i)+q_v)*Deltatau;
end
% Determine the index of the new ambient layer.
for i=1:step
    if zz(i) > zz_new && zz(i+1) < zz_new
        i_new = i;
        break
    end
end

% Rewrite the layers depth and density arrays to account
   for the new layers.
zz_temp = zz;
clear zz;
if zz_new < 0 && abs(zz_new-zz_temp(i_new))>1e-3
    if i_new > 1
        zz = [zz_temp(1:i_new) zz_new zz_temp(i_new+1:step
           +1)];
    elseif i_new == 1
        zz = [zz_new zz_temp];
    end
    clear zz_temp;
    if zz(1) < -1e-6
        zz = [0 zz];
        step = step+3;
        delta_temp=delta;
        clear delta;
        delta(1)=0;
        delta(2)=0;
        for i=1:step-3
```

```
            delta(i+2)=delta_temp(i);
        end
        delta(step)=delta(step-1)+f(step-3)/Q(step-2);
    else
        step = step+2;
        delta_temp=delta;
        clear delta;
        delta(1)=0;
        for i=1:step-2
            delta(i+1)=delta_temp(i);
        end
        delta(step)=delta(step-1)+f(step-2)/Q(step-1);
    end
else
    if zz_temp(1) < -1e-6
        zz = [0 zz_temp];
        step = step+2;
        delta_temp=delta;
        clear delta;
        delta(1)=0;
        for i=1:step-2
            delta(i+1)=delta_temp(i);
        end
        delta(step)=delta(step-1)+f(step-2)/Q(step-1);
    else
        step = step+1;
          zz = zz_temp;
        delta(step)=delta(step-1)+f(step-2)/Q(step-1);
    end
end
zz(step+1)=zetamin;

k=0;
flag_l=0;
if abs(zz(2)-zz(1))<Steptol
    i=2;
    k=k+1;
    zznew(1)=zz(1);
else
    i=1;
    k=k+1;
    zznew(1)=zz(1);
end
```

```
while i < step+1
    i=i+1;
    if i >= step
        break
    end
    if abs(zz(i)-zz(i+1))<Steptol
        i=i+1;
        k=k+1;
        znew(k)=zz(i);
        deltanew(k-1)=(delta(i-1)*(zz(i)-zz(i-1))+delta(i)
            *(zz(i+1)-zz(i)))/(zz(i+1)-zz(i-1));
        if i==step-1
            flag_l=1;
        end
    else
        k=k+1;
        znew(k)=zz(i);
        deltanew(k-1)=delta(i-1);
        if i==step-1
            flag_l=0;
        end
    end
end
if flag_l==0
    k=k+1;
    znew(k)=zz(step);
    deltanew(k-1)=delta(step-1);
    k=k+1;
    znew(k)=zz(step+1);
    deltanew(k-1)=delta(step);
elseif flag_l==1
    k=k+1;
    znew(k)=zz(step+1);
    deltanew(k-1)=delta(step);
end
clear zz delta
zz=znew;
delta=deltanew;
step=length(delta);
clear znew deltanew
end
```

Appendix C

Outflow volume flux expression for a non-negligible viscous dissipation in the lower opening

As mentioned in Chapter 2, in the natural ventilation context, viscous dissipation due to flow through the lower opening is usually ignored. However, for low Reynolds number flows or openings with small cross-sectional area, the viscous dissipation may become too significant to ignore. In that case, the outflow volume flux should be modified to account for the head loss, Δh_v, due to flow through the lower opening. Assuming a cross-sectional area of A, Δh_v can be modeled using the Darcy-Weisbach equation:

$$\Delta h_v = \sqrt{\pi} f_D \frac{b}{\sqrt{A}} \frac{Q_{out}^2}{4gA^2}, \tag{C.1}$$

where f_D is the Darcy friction factor (May, 2009).

At some depth between the interface and the lower boundary of the box, the hydrostatic pressure is equal inside and outside the box. This depth is known as the "neutral depth" (Linden *et al.*, 1990). Writing x_n for the vertical distance between the neutral depth and the interface depth, and using the Bernoulli's theorem we have (see

figure C.1)

$$Q_{out}^2 = 2A_1^2 g'(h - x_n + b) - 2g\Delta h_v, \tag{C.2}$$

$$Q_{in}^2 = 2A_2^2 g' x_n, \tag{C.3}$$

where A_1 and A_2 denote, respectively, the cross-sectional areas of the lower and upper openings. Because an extension to a stratified contaminated layer is straightforward (C.2) and (C.3) are, for the sake of simplicity, written for a well-mixed contaminated layer and a perfectly smooth expansion.

If the fluid is compressible, the volume flux into and out of the box must be the same, so that

$$Q_{in} = Q_{out}. \tag{C.4}$$

Eliminating x_n from (C.2) and using (C.4) gives

$$Q_{out} = \psi A^\star \sqrt{g'(h+b)}, \tag{C.5}$$

where

$$\psi = \left(1 + \frac{\sqrt{\pi} f_D b A^{\star^2}}{4A_1^{5/2}}\right)^{-1/2} \quad \text{and} \quad A^\star = \frac{\sqrt{2} A_1 A_2}{\sqrt{A_1^2 + A_2^2}}. \tag{C.6}$$

We opine that for $\left(\sqrt{(\pi)} f_D b A^{\star^2}/4A_1^{5/2}\right) < 0.01$ wherein $\psi \geq 0.95$, the inviscid approximation is not unreasonable. The Darcy friction factor for fully turbulent pipe flow is nearly independent of the Reynolds number and is only a function of the relative roughness of the pipe wall. Figure C.2, shows ψ as a function of f_D for a box with fissure depth $b = 1\,\text{m}$, and lower and upper fissures diameters $D_1 = D_2 = 0.3\,\text{m}$. Here clearly, and consistent with the discussion

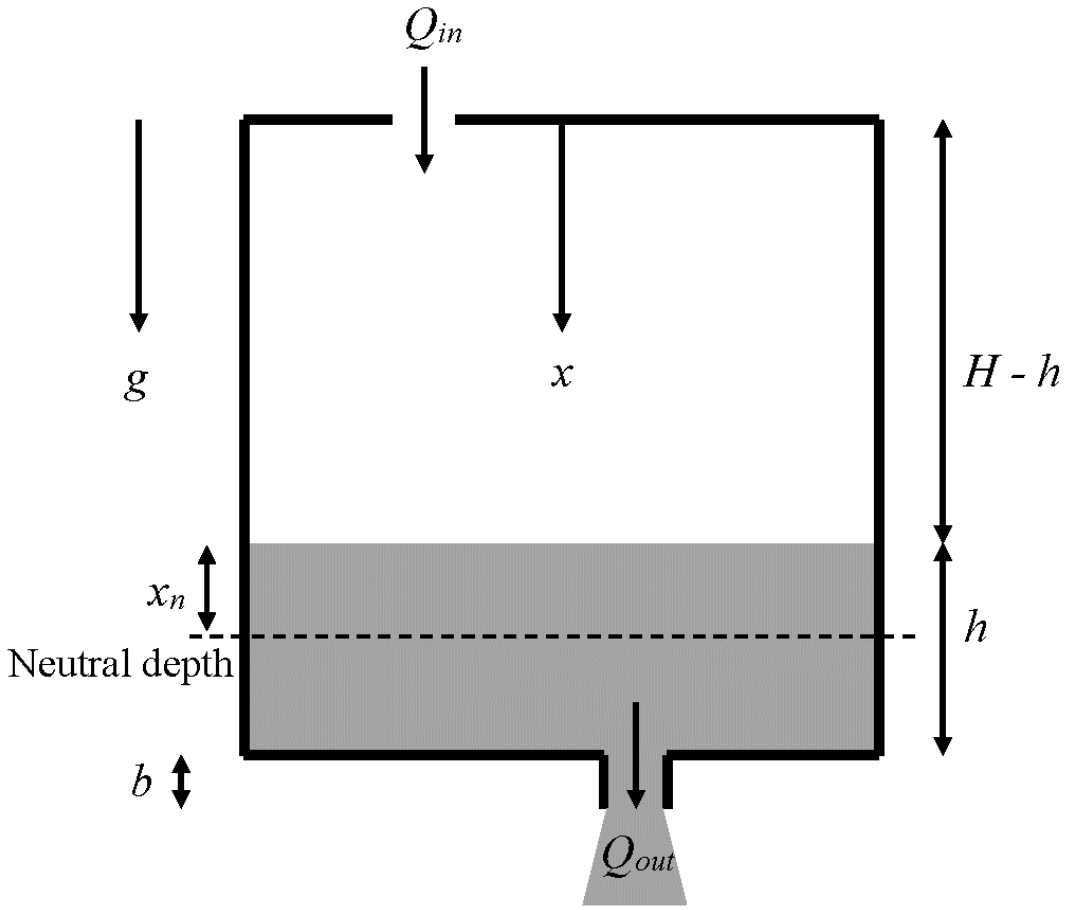

Figure C.1: Sketch of an emptying filling box flow with the location of the neutral depth indicated. The neutral depth is the depth at which the hydrostatic pressure inside and outside the box are equal.

of Chapter 2, ψ can be approximated as unity corresponding to an inviscid flow.

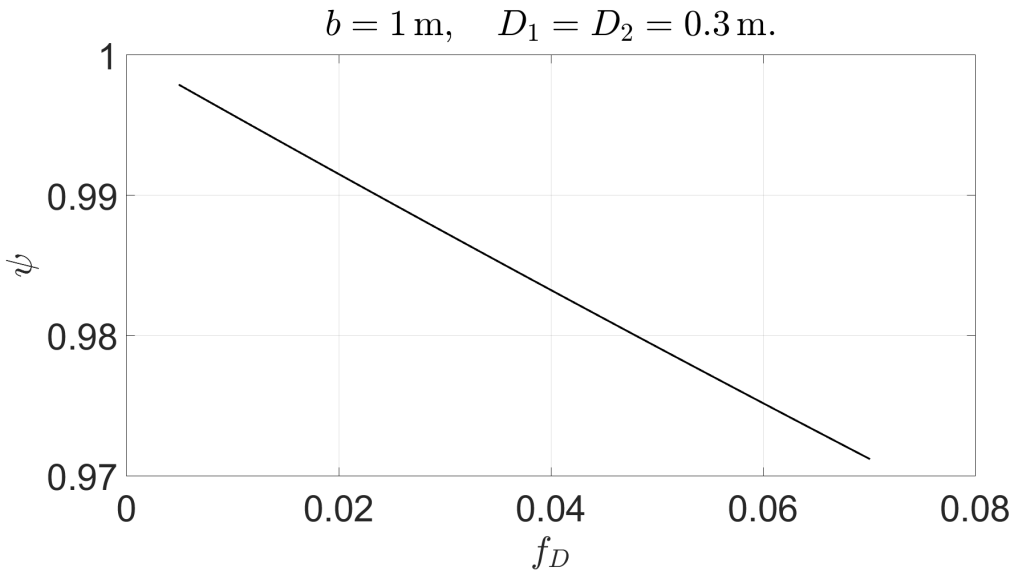

Figure C.2: ψ as a function of the Darcy friction factor, f_D.

Appendix D

Porous media emptying filling box formulation for a box with variable cross-sectional area

One of the key geometrical assumptions applied in Chapter 2 is that the cross-sectional area of the box does not change as a function of depth. This is certainly a reasonable assumption in case of architectural flows, but it's relevance to porous media geophysical flows is rather suspect. In this section, we therefore address this modeling deficiency by reviewing the equations applicable to a ventilated box containing a porous medium and having a variable cross-sectional area that changes with x.

Similar to section 2.1, we start with the equations for conservation of volume and buoyancy of the contaminated layer, i.e.

$$\frac{\mathrm{d}}{\mathrm{d}t}\left(\int_{H-h}^{H}\phi S(x)\mathrm{d}x\right) = Q_p - Q_{out}, \tag{D.1}$$

$$\frac{\mathrm{d}}{\mathrm{d}t}\left(\int_{H-h}^{H}\phi S(x)g'(x,t)\mathrm{d}x\right) = F_0 - Q_{out}g'|_{x=H}. \tag{D.2}$$

Applying Leibniz's integral rule to the left-hand side of (D.1) leads

to

$$\phi S_i \frac{\mathrm{d}h}{\mathrm{d}t} = Q_p - Q_{out}, \tag{D.3}$$

where $S_i = S(H-h)$ is the cross-sectional area of the box at the interface depth. Now, we can introduce $\bar{S} = \frac{1}{H}\int_0^H S(x)\mathrm{d}x$ as the average cross-sectional area of the box in order to rewrite (D.3) and (D.2) as:

$$\phi \bar{S}\eta \frac{\mathrm{d}h}{\mathrm{d}t} = Q_p - Q_{out}, \tag{D.4}$$

$$\phi \bar{S} \frac{\mathrm{d}I^\star}{\mathrm{d}t} = F_0 - Q_{out} g'|_{x=H}, \tag{D.5}$$

respectively, where $\eta = S_i/\bar{S}$ and $I^\star$ is the integrated buoyancy of the contaminated layer defined as

$$I^\star = \int_{H-h}^{H} \eta g'(x,t)\mathrm{d}x. \tag{D.6}$$

As before, we define the average reduced gravity of the contaminated layer as $\bar{g}' = I^\star/h$ and use (2.6) and (2.7) to rewrite (D.4) and (D.5) as

$$\phi \bar{S} \frac{\mathrm{d}h}{\mathrm{d}t} = 8\pi D\phi(H-h+x_0) - \frac{Ak_f}{\nu b}(\bar{g}'h + g'|_{x=H} b), \tag{D.7}$$

$$\phi \bar{S} \frac{\mathrm{d}(\bar{g}'h)}{\mathrm{d}t} = F_0 - \frac{Ak_f}{\nu b}(\bar{g}'h + g'|_{x=H} b) g'|_{x=H}, \tag{D.8}$$

for a point-source porous media plume, and as

$$\phi \bar{S} \frac{\mathrm{d}h}{\mathrm{d}t} = \left(\frac{36 D\phi F_0 k \Lambda^2}{\nu}\right)^{1/3} (H-h+x_0)^{1/3} - \frac{Ak_f}{\nu b}(\bar{g}'h + g'|_{x=H} b), \tag{D.9}$$

$$\phi \bar{S} \frac{\mathrm{d}(\bar{g}'h)}{\mathrm{d}t} = F_0 - \frac{Ak_f}{\nu b}(\bar{g}'h + g'|_{x=H} b) g'|_{x=H}, \tag{D.10}$$

for a line-source porous media plume. Using the dimensionless parameters introduced in (2.17), (D.7)-(D.10) can be rewritten as

$$\frac{\mathrm{d}\xi}{\mathrm{d}\tau} = \frac{\sqrt{\mu}}{\eta}\left(1-\xi+\frac{x_0}{H}\right)^k - \frac{1}{\sqrt{\mu}\eta b/H}\left(\delta\xi+\delta|_{x=H}\frac{b}{H}\right), \tag{D.11}$$

$$\begin{aligned}\frac{\mathrm{d}\delta}{\mathrm{d}\tau} =& \frac{\sqrt{\mu}}{\xi}\left[1-\frac{\delta}{\eta}\left(1-\xi+\frac{x_0}{H}\right)^k\right] \\ &+ \frac{\delta-\delta|_{x=H}}{\sqrt{\mu}\eta b/H}\left(\frac{\delta\xi+\delta|_{x=H}b/H}{\xi}\right),\end{aligned} \tag{D.12}$$

where μ is given either by (2.26) or (2.27). Hence, as long as the cross-sectional area of the box at every depth is known, (D.11) and (D.12) can be solved in order to find the depth and average reduced gravity of the contaminated layer.

Figure D.1 shows the evolution of ξ and δ for ideal point-source porous media plumes with $\mu = 5$ and $b/H = 0.1$ in a cuboid, an isosceles trapezoid prism (long side on bottom) with a base angle of $\pi/4$, and an isosceles trapezoid prism (long side on top) with a base angle of $3\pi/4$. All three geometries have the same depth and average cross-sectional area. As shown in this figure, and also figure D.2, the contaminated layer in an isosceles trapezoid prism with the long side on top has the greatest depth and the smallest reduced gravity among the three geometries. This observation can be rationalized as follows: for contaminated layers of equal depth, the contaminated fluid volume is smaller in an isosceles trapezoid with the long side on top due to the smaller cross-sectional area. Hence, the amount of discharged plume fluid available to be re-entrained into the plume is also smaller. As a result, the density of plume fluid appearing at the bottom of the box does not increase as quickly as in the other

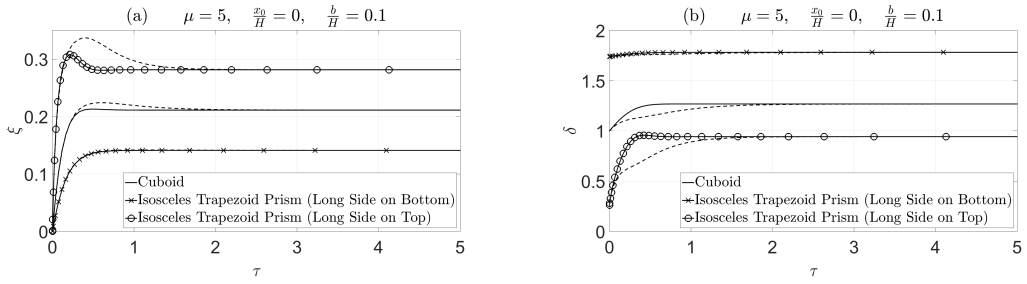

Figure D.1: Evolution of the contaminated layer non-dimensional depth (panel a) and reduced gravity (panel b) for an ideal point-source porous media plume with $\mu = 5$ and $b/H = 0.1$ for three different box geometries. The solid and dashed curves correspond to the well-mixed and approximate stratified models, respectively.

cases. However, as μ increases, the depth of the contaminated layer increases and the differences of discharged fluid volume in the three geometries decrease because the total volume of the three geometries are all the same. In the limit of very large μ (not shown), the differences become imperceptibly small.

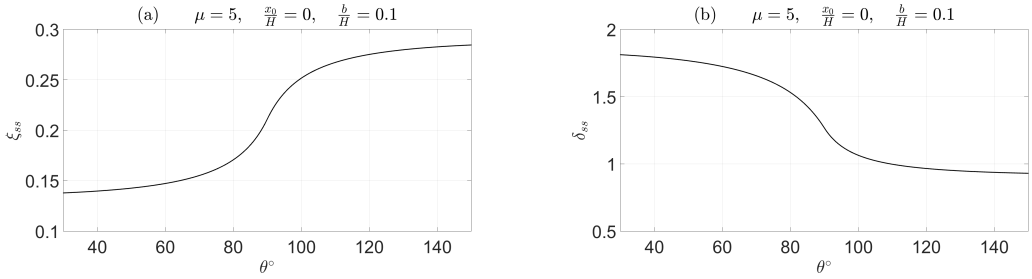

(a) (b)

Figure D.2: Steady state depth (panel a) and reduced gravity (panel b) of the contaminated layer for an ideal point-source porous media plume with $\mu = 5$ and $b/H = 0.1$ in isosceles trapezoid prisms as functions of the base angle, θ. Recall that $\theta = 90^\circ$ corresponds to the cuboid that is the focus of attention in Chapter 2.

Appendix E

Stability of second-order linear homogeneous differential equations systems with constant coefficients

In this section, we adapt the discussion of Boyce & DiPrima (2008) and present a geometric analysis in order to review different types of stability associated with systems of second-order linear homogeneous differential equation with constant coefficients. Such systems have the form

$$\frac{\mathrm{d}\mathbf{x}}{\mathrm{d}t} = \mathbf{A}\mathbf{x}, \tag{E.1}$$

where $\mathbf{A}$ is a 2×2 constant matrix and $\mathbf{x}$ is a 2×1 column vector. Substituting a generic solution such as $\mathbf{x} = \boldsymbol{\zeta} e^{rt}$ in (E.1) leads to

$$(\mathbf{A} - r\mathbf{I})\boldsymbol{\zeta} = \mathbf{0}. \tag{E.2}$$

Thus, r and $\boldsymbol{\zeta}$ are the eigenvalue and corresponding eigenvector of the matrix $\mathbf{A}$. In the analysis of systems of differential equations, critical points, defined as points with $\mathbf{A}\mathbf{x} = \mathbf{0}$, are of special importance. Assuming that $\mathbf{A}$ is nonsingular, i.e. its determinant is non-zero, $\mathbf{x} = \mathbf{0}$ is the only critical point of the system (E.1).

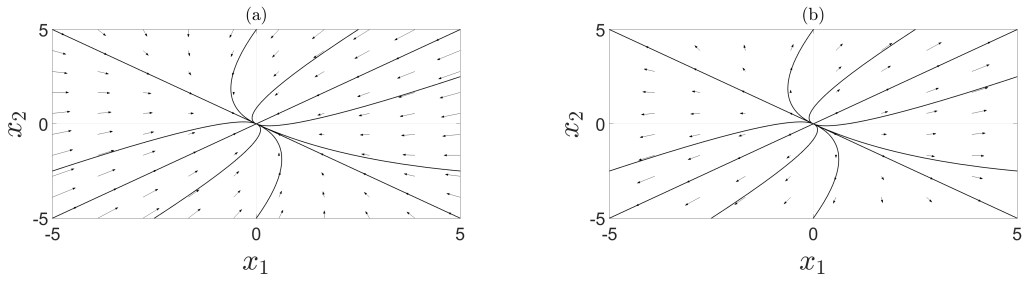

Figure E.1: The phase planes of (a) a nodal sink and (b) a nodal source.

A solution of (E.1) is a vector function $\mathbf{x} = \boldsymbol{\phi}(t)$ that satisfies the differential equations. Such a function can be regarded as a parametric representation of a curve in the x_1x_2 plane which is called the trajectory. The x_1x_2 plane is referred to as the phase plane and a representative set of trajectories is called a phase portrait.

Depending of the nature of the eigenvalues of $\mathbf{A}$, several different cases may arise. In the following, we discuss the behaviour of the trajectories for each case and categorize the differential equations accordingly.

Real unequal eigenvalues of the same sign. The general solution of (E.1) is

$$\mathbf{x} = c_1\boldsymbol{\zeta}^{(1)}e^{r_1t} + c_2\boldsymbol{\zeta}^{(2)}e^{r_2t}, \tag{E.3}$$

in which r_1 and r_2 are either both positive or both negative. If r_1 and r_2 are both negative (positive), it follows that all solutions approach (move away from) the critical point as $t \to \infty$. This type of critical point is called nodal sink (nodal source). Examples of a nodal sink/source are given in figure E.1.

Real eigenvalues of opposite sign. The general solution of

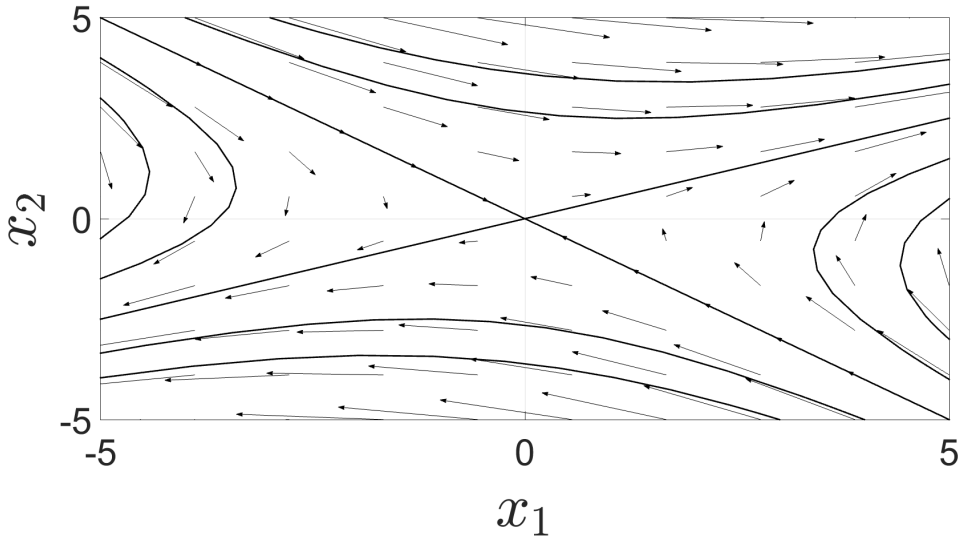

Figure E.2: The phase plane of a saddle node.

(E.1) is

$$\mathbf{x} = c_1\boldsymbol{\zeta}^{(1)}e^{r_1 t} + c_2\boldsymbol{\zeta}^{(2)}e^{r_2 t}, \tag{E.4}$$

where $r_1 > 0$ and $r_2 < 0$. If a solution starts on $\boldsymbol{\zeta}^{(1)}$, i.e. $c_2 = 0$, it remains on the line though $\boldsymbol{\zeta}^{(1)}$ for all t and because $r_1 > 0$, $||\mathbf{x}|| \to \infty$ as $t \to \infty$. Similarly, if the solution starts on $\boldsymbol{\zeta}^{(2)}$, it remains on the line though $\boldsymbol{\zeta}^{(2)}$. However, since r_2 is now negative, the solution approaches the critical point as $t \to \infty$. Because the term with the positive exponential is dominant in (E.4), for solutions starting at any distance away from $\boldsymbol{\zeta}^{(2)}$, they will, in the long time limit, approach infinity asymptotic to the line though $\boldsymbol{\zeta}^{(1)}$. The critical point is called a saddle node in this case. An example of the phase plane for a saddle node is illustrated in figure E.2.

Equal eigenvalues. Suppose that $r_1 = r_2 = r$. In this case, two subcases may arise depending on whether there are two independent

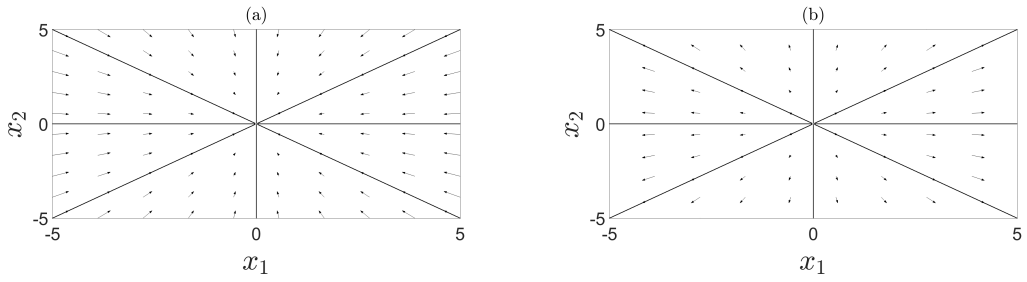

Figure E.3: The phase planes of (a) a stable star node and (b) an unstable star node.

eigenvectors or only one.

(a) Two independent eigenvectors. The general solution of (E.1) is

$$\mathbf{x} = c_1\boldsymbol{\zeta}^{(1)}e^{rt} + c_2\boldsymbol{\zeta}^{(2)}e^{rt}. \tag{E.5}$$

In this case, the ratio of x_1/x_2 is independent of t and only depends on the components of $\boldsymbol{\zeta}^{(1)}$ and $\boldsymbol{\zeta}^{(2)}$, and on the constants c_1 and c_2. Thus, every trajectory lies on a straight line though the origin and depending on the sign of r, the solution may approach or move away from the origin in the long time limit. Such a critical point is referred to as a star node. Examples of the phase planes of stable and unstable star nodes are shown in figure E.3.

(b) One independent eigenvector. The general solution of (E.1) is

$$\mathbf{x} = c_1\boldsymbol{\zeta}e^{rt} + c_2(\boldsymbol{\zeta}te^{rt} + \boldsymbol{\eta}e^{et}), \tag{E.6}$$

where $\boldsymbol{\zeta}$ and $\boldsymbol{\eta}$ are the eigenvector and the generalized eigenvector, respectively. Suppose that $r < 0$. For large t, the dominant term is $c_2\boldsymbol{\zeta}te^{rt}$. Hence, as $t \to \infty$, the trajectories approach the critical point tangent to $\boldsymbol{\zeta}$. Likewise, for large negative t, each trajectory is

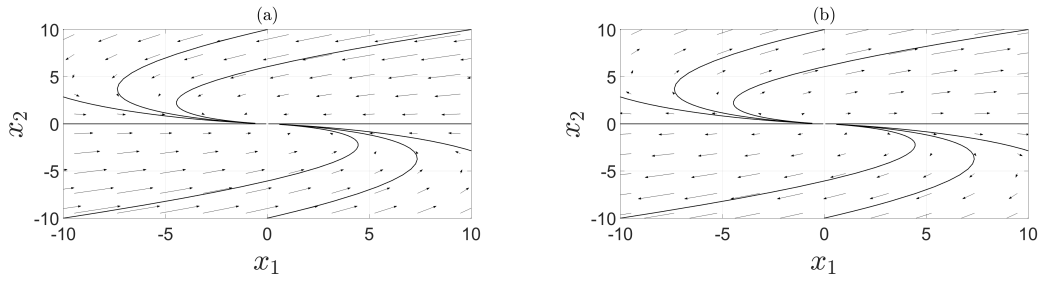

Figure E.4: The phase planes of (a) a stable degenerate node and (b) an unstable degenerate node.

asymptotic to a line parallel to $\boldsymbol{\zeta}$. Such a critical point is called a degenerate node. If r is negative, the behaviour is similar but the direction of motion is reversed. Typical phase planes of stable and unstable degenerate nodes are presented in figure E.4.

Complex eigenvalues. Suppose that the eigenvalues are $\alpha \pm i\beta$, where α and β are real with $\alpha \neq 0$ and $\beta \neq 0$. After some algebra, for a simplified case, (E.1) can be rewritten in polar coordinates as

$$r' = \alpha r, \tag{E.7}$$

$$\theta' = -\beta. \tag{E.8}$$

Integrating the above equations leads to

$$r = ce^{\alpha t}, \tag{E.9}$$

$$\theta = -\beta t + \theta_0, \tag{E.10}$$

where c is a constant and θ_0 is the value of θ when $t = 0$. According to (E.7), as $t \to \infty$, $r \to \infty$ for $\alpha > 0$ and $r \to 0$ for $\alpha < 0$. Also, the sign of β determines the direction of motion on a trajectory. If $\beta > 0$, the motion is clockwise, and if $\beta < 0$, the motion is

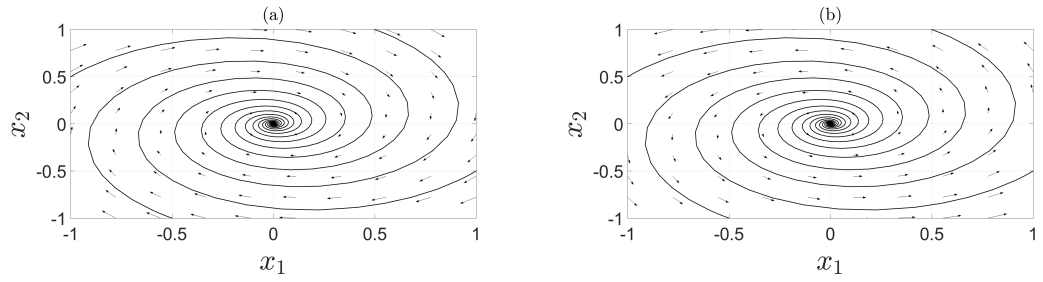

Figure E.5: The phase planes of (a) a spiral sink and (b) a spiral source.

counterclockwise. Such a critical point is called either a spiral source or a spiral sink. Examples of trajectories of a spiral sink and a spiral source are given in figure E.5.

Pure imaginary eigenvalues. In this case $\alpha = 0$ and the system of equations (E.7-E.8) reduces to

$$r' = 0, \tag{E.11}$$

$$\theta' = -\beta, \tag{E.12}$$

and consequently

$$r = c, \tag{E.13}$$

$$\theta = -\beta t + \theta_0. \tag{E.14}$$

Hence, the trajectories are circles with centers at the origin. As before, the sign of β determines the direction of motion of a trajectory. Such a critical point is referred to as a center. An example of the phase plane of a center node is presented in figure E.6.

Returning to section 2.3, if the linearized system, (2.36), has two complex conjugate eigenvalues for given μ, b/H and x_0/H, the steady state is a spiral node. Hence, an overshoot of the terminal

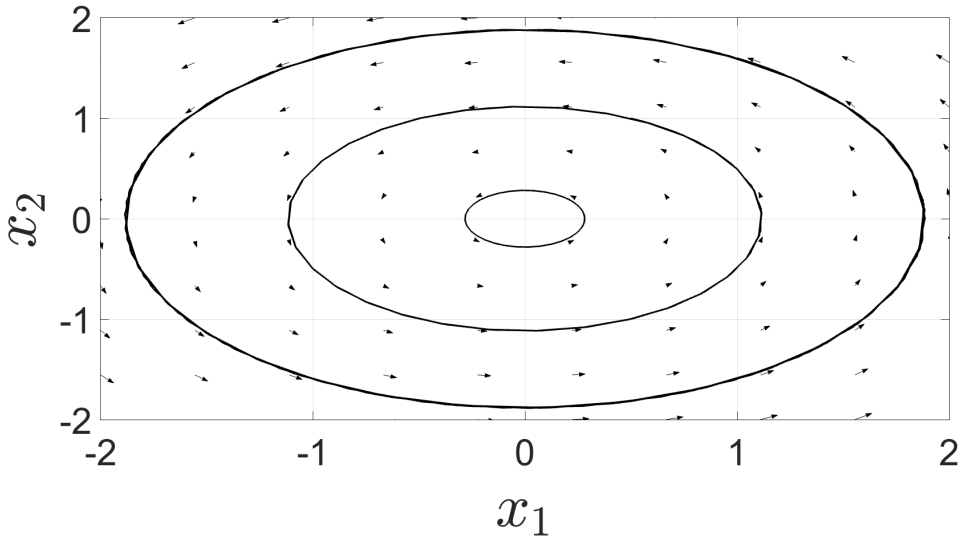

Figure E.6: The phase planes of a center.

layer depth (and also mean reduced gravity) is guaranteed.